

## Theory of Precursory Processes in the Inception of Earthquake Rupture

By J. R. Rice, Providence\*)

(With 10 figures)

### Summary

The paper reviews models for inelastic deformation processes preceding earthquake rupture in brittle, natural rock masses. The discussion is organized around three types of failure models: (i) localization bifurcations, whereby a uniform or nearly uniform pattern of deformation gives way to highly localized deformations within a fault zone; (ii) non-homogeneous deformations due to an inclusion-like zone of different mechanical properties than its surroundings, possibly representing a seismic gap, which is driven ultimately to a "runaway" dynamic instability; and (iii) a slipping region on an existing fault, which spreads on the fault plane under initially quasi-static conditions until limiting conditions for rapid shear-crack propagation are met. It is emphasized that failure conditions are sensitive to strain-softening behavior of nominally coherent rock or fault gouge, and that a general precursor is provided by the acceleration of local, by comparison to remote tectonic, deformations as instability conditions are approached. More striking precursors may arise from the presence of an infiltrating pore fluid. This may cause time-dependent surface-chemical effects, such as reductions of resistance to microcrack growth and post-fault strength recovery in compacted gouge, and also mechanical effects due to dilatant strengthening and time-dependent stiffness of elastic response at conditions intermediate between the drained and undrained limits. Some calculations of stabilization against abrupt earthquake rupture by these mechanical effects are given for the above models.

### Zusammenfassung

Die Arbeit gibt einen Überblick über Modelle für unelastische Deformationsprozesse, welche Erdbebenbrüchen in spröden natürlichen Gesteinsmassen vorausgehen. Die Diskussion erstreckt sich auf drei Typen von Bruchmodellen: (1) Lokalisationsbifurkation, wobei ein gleichförmiges oder nahezu gleichförmiges Deformationsmodell zu stark lokalisierten Deformationen innerhalb der Bruchzone führt; (2) inhomogene Deformationen auf Grund einer inklusionsähnlichen Zone mit unterschiedlichen mechanischen Eigenschaften in bezug auf die Umgebung, die möglicherweise einen seismischen Spalt darstellt, der zum Schluß zu einer „weglaufenden“ dynamischen Instabilität führt; und (3) eine Gleitregion an einem existierenden Bruch, welche sich über die Bruchebene unter ursprünglich quasistatischen Bedingungen ausbreitet, bis die Grenzbedingungen für eine schnelle Scherbruchausbreitung erreicht sind. Es wird deutlich gemacht, daß Bruchbedingungen empfindlich gegenüber Strain-softening-Verhalten von nominell einheitlichem Gestein oder Verwerfungsletten sind. Weiterhin zeigt sich, daß die Beschleunigung von — im Vergleich zur entfernten Tektonik — lokalen Deformationen bei Erreichen der Instabilitätsbedingungen ein allgemeiner Vorläufer ist. Auffallendere Vorläufer können durch die Anwesenheit von durchsickernden Porenflüssigkeiten auftreten. Dadurch können zeitabhängige chemische Oberflächeneffekte entstehen, wie zum Beispiel Reduktion des Widerstandes gegenüber Mikrorißwachstum und Wiedererlangung der Nachverfestigungsstärke in verdichteten Verwerfungsletten und auch mechanische Effekte durch dilatante Verstärkung und zeitabhängige Zähigkeit des elastischen Responses bei Zwischenbedingungen zwischen trockenen und wasserreichen Grenzbedingungen. Einige Berechnungen der Stabilität gegenüber abrupten Erdbebenbrüchen durch diese mechanischen Effekte werden für die obigen Modelle durchgeführt.

---

\*) Dr. JAMES R. RICE, Division of Engineering, Brown University, Providence, Rhode Island, U.S.A.

### Резюме

Работа дает обзор о моделях неупругих процессов деформации, которые предшествуют сейсмическим разрушениям в естественных хрупких массах горных пород. Обсуждение распространяется на три типа моделей разрушения: (1) локализованный скол, где однородная или почти однородная модель деформации ведет к сильной концентрации деформации внутри зоны разрушения; (2) неоднородные деформации на основе зоны в виде включения с отличающимися от окружающей среды механическими свойствами, которая, возможно, представляет собой сейсмическую трещину, которая в конце ведет к „убегающей“ динамической неустойчивости; и (3) зона скольжения у существующего разлома, которая распространяется на плоскость разрыва сначала в квазистатических условиях, пока не достигаются граничные условия для быстрого распространения сдвигового разрушения. Поясняется, что условия разрушения являются чувствительными относительно поведения деформация-смягчивание однородной горной породы или прослая глины. Дальше оказывается, что ускорение локальных деформаций, по сравнению с далекой тектоникой, при достижении условий неустойчивости является общим предшественником. Более заметные предшественники могут возникать за счет просачивающей поровой влаги. Таким образом могут появляться химические поверхностные эффекты, как например понижение сопротивления относительно возрастания микротрещин и повторного достижения прочности после разрушения в уплотненных прослоях глины, а также механические эффекты из-за укрепления за счет расширения и зависимой от времени жесткости упругого реагирования при условиях, лежащих между сухими и влагонасыщенными граничными условиями. Проводятся некоторые расчеты устойчивости относительно внезапных сейсмических разрушений за счет этих механических эффектов для выше указанных моделей.

### 1. Introduction

This is a review of theoretical studies of processes in natural rock masses that are preparatory to Earth faulting. As such the work attempts to contribute to the understanding of the nature and time scale of processes that may lead to discernible earthquake precursors, be these effects on seismic or electrical transmission properties in pre-faulted rock, or on accelerating fault creep slippage or strain and tilt at ground surface.

An attempt is made to organize discussion on the basis of mechanically consistent models of the failure process, implemented with constitutive descriptions that seem to incorporate the principal features of natural rock behavior. Of course, such models involve enormous uncertainty, arising from imprecise knowledge of the stress levels and distributions prevailing in earthquake regions, of the heterogeneity of rock properties, and proper boundary conditions for representation of tectonic loading. For example, is the 10 to 100 bar stress-drop range frequently cited representative of a major or only a very small part of ambient shear-stress levels? Does previous faulting dominate subsequent response and cause all non-elastic deformation to be localized in a fault zone, or is more diffuse deformation typical? Further, the effects of geometric size and of very long times at ambient temperatures remain poorly understood in the generalization to field conditions of laboratory-based studies of inelastic rock deformation and friction. A natural fault of 5 km diameter is larger by a factor of  $10^5$  or so in linear dimensions than faults produced in typical laboratory triaxial tests, and a representative laboratory strain rate of  $10^{-5}/s$  is very fast indeed compared to tectonic strain rates of  $10^{-13}/s$  (estimated from assumed shear-stress rate of 1 bar/yr.). Also, laboratory studies to date have still not very fully documented some elements of constitutive response that seem important to failure models. These include post-peak-

strength behavior, response to general non-proportional stress increments, creep-like processes arising, for example, from the exposure of microcracks to a surface-reactive environment such as groundwater or humid air, and long-term processes of strength recovery by crack healing, cementation reactions, etc.

In the circumstances, one reaction may be to abandon theory as premature and, indeed, I believe that there is little point in studying overly detailed models of the failure process at this time. But there is a definite need for a broad understanding of generic classes of failure models, under the range of conditions that can be plausibly generalized from field and laboratory studies, as a basis for interpretation of precursory observations and for the identification of critical "signatures" of different models, that might aid in discriminating among the range of plausibly assumed conditions.

## 2. General discussion

Subsequent chapters of the paper review the results of specific models for the failure process and attempt to draw conclusions concerning the type of precursory behavior that may be exhibited and physical processes that may set its time scale. In general all models considered involve some degree of non-elastic response, typically extending to the strain-softening regime prior to rupture, and a very general precursor is provided by the acceleration of local deformation that is predicted, even on the basis of rate-independent constitutive models, as tectonic stresses build gradually toward levels for the earthquake instability. But it is seen that additional and sometimes far more dramatic precursory time effects are predicted when the presence of an infiltrating pore fluid is considered. These arise partly from mechanical interactions of pore fluid with the rock mass in the form of dilatant strengthening and Biot-like time dependence of elastic response at conditions intermediate between short-time (undrained) and long-time (drained) elastic deformation. They arise also from surface-chemical effects on microcrack growth in long-term stress corrosion cracking, and on processes of time-dependent strength recovery in fault gouge.

Some general considerations, introductory to the specific analyses outlined later, are discussed in the following sections.

### 2.1. Constitutive description of brittle rock deformation and frictional response

Here the emphasis is on the macroscopically inelastic deformation of rock in the brittle range, arising from the nucleation, frictional slippage on, and growth (and, possibly, healing) of microcracks opened by internal stress concentrations, e.g., at the border of a closed fissure sliding with frictional resistance or at some other internal heterogeneity. A good review of experimental studies, mostly in the "triaxial" test, is given in the recent edition of JAEGER and COOK [12]. Further, while seldom studied experimentally, the stiffness of the material in stress response  $d\sigma_{ij}$  to strain increments  $d\varepsilon_{ij}$ , having a wide range of directions in strain space is important, for example, to the determination of stability against shear localization of a homogeneous, or nearly so, pattern of straining. In addition, the post-peak response of rock masses and of fault zones enters critically into all the failure models considered, although experimental

studies are often terminated earlier, sometimes by the dynamic instability that arises very near peak from inadequate stiffness of the testing apparatus. Important exceptions are the studies of WAWERSIK and co-workers [40], [41]. Further, models dealing with the mechanical interaction between the rock and a pore fluid are strongly sensitive to the extent of dilatancy accompanying shear (e.g., BRACE et al. [7]; BRACE and MARTIN [6]) and deformation-induced alteration of pore fluid permeabilities.

It has been noted that long-term surface-chemical interactions of fissured rock and pore water allow the possibility of time-dependent crack growth at sufficiently high stress levels and, in materials with rather flat microcrack surfaces, crack healing at low enough stress levels. This observation encourages the view, in development of constitutive relations, that the microcrack distribution not be regarded as being uniquely determined by the stress history, but rather that it and the stress be regarded as independent variables on which the strain depends, with there being an additional *kinetic* relation, to complete the constitutive description, expressing the rate of growth of some measure of the microcrack network in terms of the current stress and microcrack distribution.

Also, when it is appropriate to regard the non-elastic deformations as localized in a fault zone, it is necessary to have constitutive descriptions of the relative sliding and opening displacements across the fault. There has, thus far, been rather little study of appropriate relations, although the strength limits and degradation of strength for small amounts of relative motion are important for setting conditions under which a slipping region along a fault can be expected to propagate in the form of a macroscopic shear crack. In this connection, a promising approach to the description of fault strength and deformation has been developed recently by BARTON [3], who emphasizes the important interrelations between classical friction notions and strength properties of nominally coherent rock specimens, the latter representing properties of roughness protrusions which must be deformed or uplifted to allow relative motion. In addition, recent studies by DIETERICH [10] address the displacement and speed dependence of frictional slippage in fault gouge along nominally smooth surfaces, relating friction at low speeds to his earlier studies (cf. [9]) of time-dependent strengthening on a stationary fault.

## 2.2. Types of failure models

With reference to Fig. 1, at least three generically different concepts of the inception of earthquake failure may be envisioned, and it seems probable that actual faulting may involve elements of each.

### 2.2.1. *Localization of previously homogeneous deformation*

Fig. 1a depicts a region of material which has been deformed homogeneously, or nearly homogeneously, into the inelastic regime to a point at which certain critical conditions are met at which the deformation pattern bifurcates into a highly localized "shear band". Corresponding behavior has been widely observed in initially coherent laboratory specimens, not only of geological materials but also of ductile metals and polymers, although the relevance of the concept to large regions of the Earth is problematical, since these may have deformation fields which are strongly localized from the start in zones weakened by previous faulting. Then, only with the intervention of

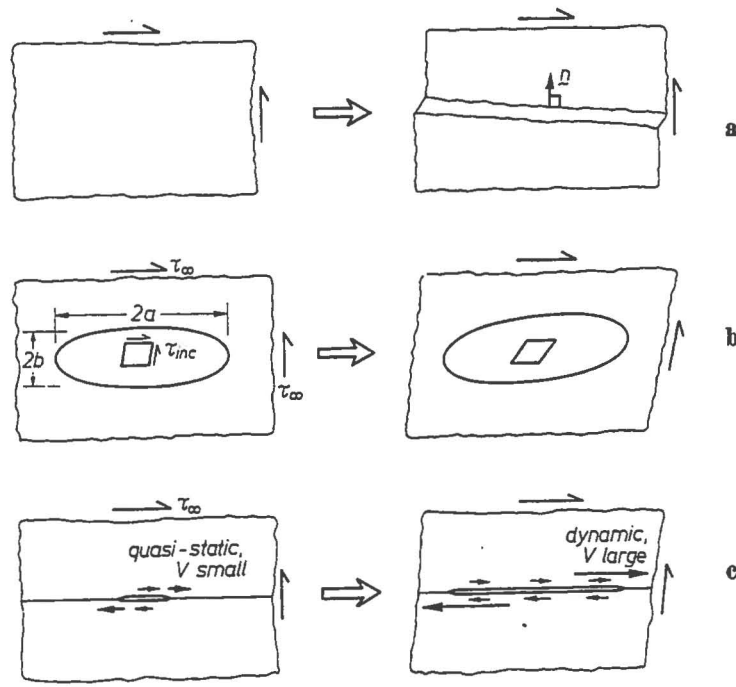


Fig. 1. Types of failure models. **a** Localization of previously uniform or nearly uniform deformation; **b** deformation of "inclusion" of different mechanical properties; "runaway" instability based on strain softening of inclusion and elastic unloading stiffness; **c** isolated region of slippage on pre-existing fault, spreading quasi-statically at small speed  $V$ ; process becomes unstable, slipping region spreads dynamically at large speed

some mechanism of re-healing or cementation of the ruptured surface would the localization concept of Fig. 1a apply to subsequent faulting. MYACHKIN et al. [17] propose a localization mechanism of this kind, involving the gradual concentration of initially diffuse and somewhat time-dependent growth of microcracks into a narrow fault zone, as a viable mechanism for the onset of faulting.

The theory of deformation localization originated with HADAMARD's well-known 1903 study of stability of finetely deformed elastic solids, and was extended to non-elastic materials in the early 1960's by THOMAS, HILL, ODE, and MANDEL. A comprehensive review of the subject and derivation of critical conditions for a wide range of rate-independent constitutive models is given by RICE [25]. The critical conditions for localization are equivalent to those at which the field equations governing continuing increments of deformation lose ellipticity and admit characteristic surfaces, along which the incipient localization occurs. The conditions are also those for which the least speed of deformation wave propagation in any direction has fallen to zero; disturbances do not then spread, and in this sense the localization zone is sometimes referred to in HADAMARD's terminology as a "stationary discontinuity". RUDNICKI and RICE [32], in work further extended by RUDNICKI [29], have derived localization conditions for two inelastic constitutive models inclusive of frictional and dilatant behavior representative of brittle rock, and these results will be discussed subsequently.

It is well to understand that such localization conditions, in non-elastic solids, are not necessarily indicative of dynamic instability. Indeed, it is well known experimentally that specimens can sometimes deform in a quasi-stable manner (under overall

displacement control) after one or several localized bands have emerged. Further, according to theoretical predictions such localizations can occur with either a negative or positive rate of strain hardening, the latter favored by deformation states close to plane-strain conditions. It has been argued (RUDNICKI [30], [31]) that their casual association with the peak-strength state in standard triaxial tests may be an artifact of inadequate stiffness of the testing apparatus. Indeed, tests in the stiff triaxial apparatus of WAWERSIK and FAIRHURST [41] and WAWERSIK and BRACE [40] show evidence for macroscopically uniform deformation well into the strain softening, post-peak regime before localization.

### 2.2.2. *Local instability of inhomogeneous zone*

By contrast to the localization concept of Fig. 1 a, it seems more generally applicable that the pre-failure process will be dominated by large-scale heterogeneities of mechanical properties that remain as a consequence of previous faulting. Then a model such as in Fig. 1 b may be more appropriate. This model postulates that a region may have properties distinctly different from its surroundings, thus causing a non-uniform distribution of stress. The region is idealized as an ellipsoidal "inclusion" following RUDNICKI [31], and within it properties are taken as locally uniform and different from the surroundings. RUDNICKI envisions the inclusion as representing a zone that has been "weakened" by previous faulting, and which is deformed to conditions at and beyond its peak-stress level while the surroundings remain nominally elastic.

However, the same concepts would apply, and may be somewhat more pertinent, if the zone is taken as a region which has, on average, not faulted nearly so much as the material to the sides of it in recent geologic history, so that the zone is "misfitting" and must support a stress well in excess of that acting in the remote surroundings. This large local stress drives the material of the inclusion toward and beyond peak-strength conditions while the surroundings, as in RUDNICKI's weakened-zone interpretation of the model, remain nominally elastic. Thus, what is being described may be thought of as the impending instability of a "seismic gap" zone.

The earthquake appears as a dynamic "runaway" instability in this model. As the remote stress  $\tau_\infty$  is increased by tectonic processes there are corresponding increases of the stress  $\tau_{inc}$  within the inclusion. Finally, the peak-strength condition is reached (this does *not* generally mark instability), and the inclusion enters the strain-softening range as  $\tau_\infty$  continues to increase. Ultimately, a sufficiently negative rate of strain softening is reached so that the slope of the inclusion stress-strain relation just equals the elastic unloading stiffness of the surroundings and dynamic instability follows.

It will be seen from the more detailed analysis to follow that there is a considerable hastening of the strain rate within the inclusion over the remote tectonic strain rate as critical conditions are approached, but whether this effect alone is sufficient to give observable precursory effects on acceleration of nearby surface tilt and strain is not clear. As will also be discussed, mechanical interactions between the deforming rock mass and its pore fluid would seem to allow more dramatic effects.

### 2.2.3. *Destabilization of quasi-static fault slippage*

Finally, in Fig. 1 c we see a model in which a well-developed fault plane is postulated, and it is considered that tectonic motions are accommodated by relative slippage on this plane of a kind that is not uniform but, rather, more or less episodic. Due

to local stress build-ups certain regions of the fault begin to slide and, due to the stress concentration at its edges, the slipping region spreads outwards in a shear-crack-like mode. Depending on the non-uniformities of driving stresses and resistance, and possibly on certain rate-dependent mechanisms of local strengthening by increasing slippage rate, it is considered that the fault can spread outwards at a very slow speed under essentially quasi-static conditions. But there will, in general, also exist configurations of the slipping region for which no continuing quasi-static fault spreading can exist, without reductions in the remotely imposed deformation, and the system is then unstable. The slipping region spreads dynamically at a high speed  $V$  until some new equilibrium distribution of slippage is reached.

By assuming a strain-softening relation between shear stress and relative displacement across a slipping surface, in analogy to "cohesive zone" models for tensile cracks, PALMER and RICE [22] demonstrated that shear-crack-like configurations of slip surfaces can be found and showed that the propagation conditions could be phrased as the attainment of a critical "fracture mechanics" type of energy release rate, at least when the zone of active strain softening is of small linear extent. Similarly, NASON and WEERTMAN [19] observed that the slip-offset profiles of quasi-static creep events on the San Andreas system, typically spreading with  $V = 1$  to 10 km/day, were consistent with the postulate of a shear resistance having an upper yield strength for the onset of slip, followed by strain softening with continuing slip.

STUART [36] recently adopted this model and postulated a distribution of strength with depth for a long transform fault such that the upper yield strength increases smoothly with depth to a maximum value and then decreases. By solving numerically the anti-plane shear boundary-value problem appropriate to imposed remote tectonic displacements, he demonstrates that regimes of "fault creep" result, with a time scale proportional to that of tectonic loading, and with overall slippage prevented by the stronger fault portions at depth. These quasi-static motions of the boundary of the slip region give way finally to a dynamic instability, analogous to what is illustrated in Fig. 1 c. STUART shows that accelerating creep deformations occur at the surface, near its intersection with the fault trace, as instability conditions are approached.

In addition to requiring strain softening with deformation, the model also must assume that some mechanism for strength recovery exists if the process is to be repeated over again. In this regard, DIETERICH [9] has demonstrated that the static frictional resistance of fault surfaces in stationary contact with gouge layers between them, increased in an approximately logarithmic manner with time over a wide range of normal stresses (20 to 850 bar), increasing by 1 to 2% for each factor of 10 increase in contact time.

### 2.3. Mechanical effects of an infiltrating pore fluid

Pore fluids infiltrating a rock mass have the important possibility of lending initial stability to the rock as critical conditions are approached. This can allow failure to take place less abruptly, on a time scale determined by pore fluid diffusion, and there are obvious implications for the generation of discernible short-term precursors effects. The effects arise from two sources.

### 2.3.1. Dilatant hardening

First, because rock masses and fault zones are typically dilatant when sheared into the near-peak and strain-softening regimes, suctions are induced in the pore fluid when the time scale of deformation is sufficiently short by comparison to diffusion times, and the corresponding increase in "effective stress",  $\sigma - p$ , transiently augments the frictional resistance of the rock. This is REYNOLDS' phenomenon of dilatant hardening; its relevance to seismic sources has been noted by FRANK [11], and it has been studied experimentally by BRACE and MARTIN [6].

There would appear to be three possible precursory effects of dilatancy. First, as suggested above, the failure instability may be less abrupt, so that there is a period of accelerating but still essentially quasi-static deformation that may lead to discernible strain or creep slippage accumulation. With reference to the spreading slip region of Fig. 1 c, RICE and CLEARY [26] estimated the fluid suctions that would be generated by dilatancy in the rupturing region at the moving edge of the slip zone, and pointed out that these would increase the effective energy supply rate required for fault propagation (see RICE [23] for a more detailed analysis in connection with slip surface propagation in landslides of overconsolidated clay). Also, RUDNICKI [30] has given a preliminary analysis of dilatancy effects in transiently stabilizing the runaway instability of the inclusion model of Fig. 1 b.

The second possible effect of dilatancy is the generation of a regional lowering of pore pressures as accelerating deformations accumulate in the incipient focal region. For example, SUNDARAM et al. [37] suggest on the basis of pore pressure alterations in laboratory stick-slip events that accurate short-time pressure measurements be made in wells for detection of precursory signals.

Finally, a third possible effect of dilatancy, and the one which has received most recent attention, relates to NUR's [21] suggestion that dilatancy may involve the opening of a network of cracks under conditions for which a large portion of the crack space is either dry or filled with water vapor rather than liquid water. NUR proposes that this crack opening and subsequent refilling of crack space, as fluid flows in from afar to alleviate the local suction, is consistent with a precursory reduction followed by an increase of the seismic  $V_p/V_s$ -ratio (see also SCHOLZ et al. [34]; WHITCOMB et al. [42]). This proposal has attracted a great deal of attention and, just as dilatancy has been proposed as a source of  $V_p/V_s$ -anomalies, so also does it seem to be rather commonly assumed that the *absence* of a  $V_p/V_s$ -anomaly before an earthquake implies the *absence* of pre-failure dilatancy. This is plainly invalid reasoning. The NUR mechanism assumes not only that there is dilatancy but that the suction field induced by this dilatancy is strong enough to open appreciable numbers of cracks in which water, if present, is not present in a fully liquid state. This implies very strong dilatant effects, and it must be realized that far weaker dilatant suctions, leaving all pore fluid in liquid form, could have very significant precursory effects along the lines of the first and second mechanisms mentioned above.

It is to be realized also that  $V_p/V_s$ -anomalies, when they are observed, need have no connection with the presence of pore fluids. Indeed, MYACHKIN et al. [17], [18] seem to view the processes preceding instability in terms rather similar to what is implied by the localization picture in Fig. 1 a, applied to a dry rock mass. They envision that large-scale non-elastic deformations take place, without any initially strong

concentration of deformation into a shear zone, opening up a network of cracks and lowering  $V_p/V_s$ . It is then further assumed that a range of strain-softening behavior occurs and that in this range the deformations gradually localize into a narrow shear zone under decreasing stress, so that cracks close in regions away from the fault plane and  $V_p/V_s$  increases again. A similar proposal was made by STUART [35]. This mechanism would not seem to be in conflict with theoretical predictions (RUDNICKI and RICE [32]) or with experiments (WAWERSIK et al. [40], [41]), which suggest that in deformation states similar to axi-symmetric compression, appreciable strain softening can occur before localization. But it should be realized also that at least according to the theoretical models, localization will occur quite early in the post-peak regime or, in favorable circumstances, even with positive strain hardening, when the pre-failure deformation field approximates more closely to "plane strain" conditions (RUDNICKI and RICE [32]; RICE [28]). Indeed, this observation would seem pertinent to the evaluation of all models, whether dry or wet, that envision some large-scale region of the Earth that deforms well into the post-peak regime. Such may not be possible without localization in overall deformation fields of plane-strain type.

### 2.3.2. *Biot-like time-dependent elasticity*

The dilatant hardening effects just discussed involve an essentially non-linear interaction between shear deformation and pore pressure alterations. But there are also significant possibilities for fluid-induced stabilization of rupture processes that derive from the purely linear behavior of a fluid-infiltrated elastic solid as described by the BIOT [4] theory. To understand these effects it is important to realize, as emphasized in recent studies by the author and co-workers (RICE and CLEARY [26]; RICE and SIMONS [28]; RICE et al. [27]), that for short-time stress alterations the material responds in an "undrained" manner (i.e., no alteration of local fluid mass content) and is elastically stiffer, for all deformations except pure shear, than when the material responds to long-time stress alterations, in which case "drained" conditions (i.e., no alteration of local pore pressure) result.

Indeed, the critical strain-softening slope for instability of an inclusion as in Fig. 1 b is sensitive to the elastic unloading stiffness of the surroundings (RUDNICKI [31]); a more negative softening slope can be sustained for stiff than for less stiff surroundings. Thus, as remarked by RICE et al. [27], *abrupt* instability will not occur when the critical condition based on the long-term drained elastic properties of the surroundings are met, because the hastening deformations that follow this condition elicit a shorter-time response with stiffness which can approach that for the fully undrained state. Similar effects were noted by BOOKER [5]. The implication is that failure will not generally occur abruptly when critical conditions based on drained elastic properties are met, although failure is then inevitable and proceeds on a time scale controlled by fluid diffusion.

Similarly, the critical condition for unstable shear-crack-like extension of an isolated slipping region as in Fig. 1 c is also sensitive to the elastic stiffness of the surroundings. For example, the simplest fracture mechanics model for the instability (RICE and CLEARY [26]) would require that the stress intensity factor  $k$ , which characterizes the strength of the local elastic shear-stress concentration at the fault tip and is proportional to the excess of the remote shear stress  $\tau_\infty$  over the frictional resistance  $\tau$

within the slipping region, reach the critical value

$$k_{\text{crit}}^2 = \frac{2G}{1 - \nu_e} \mathcal{G}_{\text{crit}}. \quad (1)$$

Here  $\mathcal{G}_{\text{crit}}$  is the critical fracture mechanics energy absorption rate at the tip for fault extension,  $G$  is the elastic shear modulus, the same under drained or undrained conditions, and  $\nu_e$  is the effective elastic Poisson ratio, called  $\nu$  for drained and  $\nu_u$  for undrained conditions. Of course  $\nu_u \geq \nu$ , since the undrained response is stiffer, and this means that  $k_{\text{crit}}$  is larger for undrained than for drained conditions. Thus when critical conditions based on drained properties are reached, the fault does not immediately become unstable but, similarly to the case with the inclusion model, a period of accelerating but initially quasi-static creep extension of the fault begins and leads ultimately to dynamic instability.

In fact, a more precise analysis of the problem by RICE and SIMONS, based [28] on a solution of the fully coupled BIOT elastic deformation-diffusion equations for steady shear-crack advance in a fluid-infiltrated solid, suggests that even larger stabilizing effects occur than suggested by the simple argument above. These effects arise because an effectively drained region near the fault tip, present even when the overall response is nominally "undrained", is shielded somewhat from the full stress concentration by the contrast of its elastic response stiffness with that of its surroundings.

A good index of the size of these effects is the difference between  $\nu_u$  and  $\nu$  by comparison to unity. RICE and CLEARY [26] gave a table of values based on experimental data. A further perspective is provided by the calculations of BUDIANSKY and O'CONNELL [8] of the elastic properties of rock containing an array of flat crack-like penny-shaped pores of radius  $a$  and of number  $N$  per unit volume. For simplicity their results appropriate to a small crack density are used, ignoring interactions, in which case the drained ("dry" in their terminology) bulk modulus  $K$  and shear modulus  $G$  are given by

$$K/K_s = 1 - \frac{16(1 - \nu_s^2)}{9(1 - 2\nu_s)} Na^3, \quad (2)$$

$$G/G_s = 1 - \frac{32(1 - \nu_s)(5 - \nu_s)}{45(2 - \nu_s)} Na^3. \quad (3)$$

Here the quantities with subscripts  $s$  refer to properties of the solid phase. Further, when the crack-like pore spaces are fully infiltrated with a substance having bulk stiffness similar to liquid water, BUDIANSKY and O'CONNELL observe that the cracked solid responds to purely hydrostatic stress with a bulk modulus essentially identical to that of the solid, so the undrained bulk modulus is  $K_u = K_s$  in the circumstances. Since the ratios  $K/G$  and  $K_u/G$  suffice to determine  $\nu$  and  $\nu_u$ , respectively, one may calculate these from the above formulae, and the results for  $\nu_s = 0.25$  are shown in Table 1.

The last line corresponding to a crack density parameter 0.20 may be outside the range of validity of the non-interacting crack model; the full BUDIANSKY and O'CONNELL plots of  $K/K_s$  ( $\bar{K}/K$  in their notation) against  $Na^3 (= \epsilon)$  seem to exhibit some non-linearity in the range of larger  $\epsilon$  in the table. The last three columns indicate the corresponding ratios of elastic unloading stiffness of the surroundings for undrained and drained conditions, as discussed above in connection with fault stabilization by pore fluids.

Table 1. Drained ( $\nu$ ) and undrained ( $\nu_u$ ) POISSON ratios for cracked rock as function of the crack density parameter  $Na^3$ . The last three columns give the ratio of the effective elastic stiffness of the surroundings for undrained conditions to that for drained conditions, for: (i) a narrow elliptical inclusion or crack sheared under plane-strain conditions, (ii) a narrow axi-symmetrical ellipsoidal inclusion or penny-shaped crack under shear, and (iii) a spherical inclusion under shear loading

$Na^3$	$\nu$	$\nu_u$	(i) $\frac{1-\nu}{1-\nu_u}$	(ii) $\frac{(1-\nu)(2-\nu_u)}{(1-\nu_u)(2-\nu)}$	(iii) $\frac{(4-5\nu)(7-5\nu_u)}{(4-5\nu_u)(7-5\nu)}$
0	0.25	0.25	1.00	1.00	1.00
0.10	0.19	0.28	1.12	1.07	1.08
0.15	0.14	0.30	1.22	1.12	1.15
0.20	0.05	0.31	1.38	1.20	1.24

For example, as RUDNICKI [31] remarked based on the ESHELBY solution for ellipsoidal inclusions, a uniform shear stress  $\tau_{inc}$  and shear strain  $\gamma_{inc}$  (i.e., angle change between initially perpendicular line elements) are induced within a locally homogeneous inclusion as in Fig. 1 b, whether of linear or non-linear material, embedded in an isotropic elastic solid subjected to a remotely uniform shear stress  $\tau_\infty$ . The relation between the mismatch of the stress and strain fields, between the inclusion and the remote surroundings, is independent of inclusion properties and has the form

$$\tau_\infty - \tau_{inc} = (G/\xi_e) (\gamma_{inc} - \tau_\infty/G), \quad (4)$$

where  $\xi_e$  is the following function of the effective elastic POISSON ratio  $\nu_e$  and the semi-major axis  $a$  and semi-minor axis  $b$  of the ellipsoid:

$$\xi_e = \frac{(1-\nu_e)a}{b} \quad (\text{narrow elliptical inclusion in plane strain}), \quad (5)$$

$$\xi_e = \frac{4(1-\nu_e)a}{\pi(2-\nu_e)b} \quad (\text{narrow axi-symmetrical ellipsoidal inclusion}), \quad (6)$$

$$\xi_e = \frac{2(4-5\nu_e)}{7-5\nu_e} \quad (\text{spherical inclusion}). \quad (7)$$

(The second result corrects a formula given by RUDNICKI [31].)

The elastic unloading stiffness may be calculated as the derivative  $\partial\tau_{inc}/\partial\gamma_{inc}$  in the above expression, holding  $\tau_\infty$  fixed, and hence is equal to  $-G/\xi_e$ . Accordingly, the ratio  $(1/\xi_u)/(1/\xi)$  is the ratio of undrained to drained stiffness, and it is this parameter which appears in the last three columns of Table 1. Obviously, the strength of the stabilizing effect is strongly sensitive to the effective crack density in rock surrounding the region which is about to rupture.

#### 2.4. Surface-chemical effects of pore fluids

There are significant surface-chemical effects of water on the strength of quartz-based rocks (e.g., MARTIN [15]; SCHOLZ [33]; SWOLFS [38]; MARTIN und DURHAM [16]). The effect arises from the time-dependent growth of microcracks, and corresponding growth of macrocracks in technological ceramics and glasses in moist environments has been widely studied in recent years (e.g., WIEDERHORN [43]; WACHTMAN [39] for a review). Indeed, SWOLFS [38] cites the chemical similarity between silica glass and quartz-based rock, and notes that both show similar strength degradation when results

in vacuum or dry air are compared to those in water, to argue that the phenomenology of crack growth in glass may have a close resemblance to that in quartz rocks. This is verified, e.g., by studies of SCHOLZ [33] and MARTIN and DURHAM [16], but the studies in quartz have not yet been carried out with as much attention to the mechanical characterization of the crack-tip state.

In contrast, for several glasses the process of moisture-assisted crack growth has now been studied as a function of the tensile stress intensity  $k_I$ , at speeds  $V$  ranging from  $10^{-7}$  mm/s up to  $10^{-1}$  mm/s and larger (e.g., WACHTMAN [39]). Over this range the stress intensity factor doubles, approximately, from 0.3 to 0.4  $\text{MN m}^{-3/2}$  at the low speed to 0.6 to 0.7  $\text{MN m}^{-3/2}$  at the higher. Also,  $V$  for a given  $k_I$  increases with temperature (below the glass transition), and with moisture content of the surrounding air, being higher yet for liquid water than for air of maximum humidity. Fig. 2a is redrawn from results on glass in liquid water at room temperature, although details of the plateau are estimated from results in fully humid air.

Typically, the function  $V(k_I)$  divides into three regimes. There is a high  $k_I$ -regime (Regime 3) in which environmental effects do not seem significant and  $V$  is rapid, a lower  $k_I$ -regime (Regime 2) in which environmental effects are present but  $V$  is limited by the time required for transport of the embrittling species to the crack tip, and finally a Regime 1, which corresponds to low values of  $k_I$ . In Regime 1,  $V$  increases exponentially with  $k_I$ , although sometimes there is evidence for a threshold level

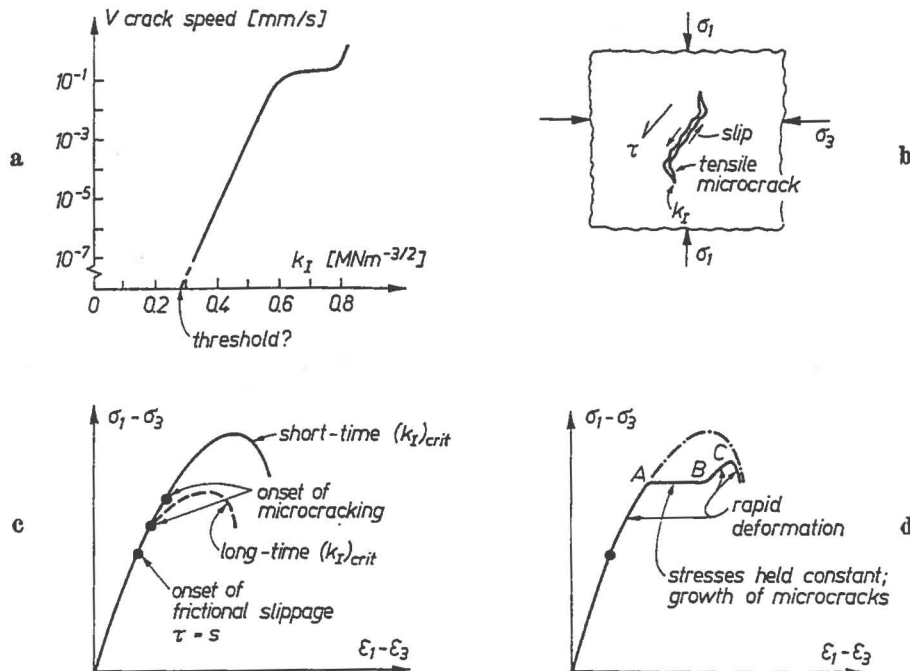


Fig. 2. a Crack growth in glass in liquid water, redrawn from plots of WIEDERHORN [43] and WACHTMAN [39]; b tensile microcracks initiated from the tip of a closed fissure slipping under frictional resistance  $s$ ;  $\tau$  is resolved shear stress and  $k_I$  is approximately proportional to  $\tau - s$  for a very short tensile microcrack; c stress-strain curves; solid curve for rapid deformation corresponds to  $k_I$  at its short-time "critical" value; dashed curve for much slower deformation corresponds to long-time "critical" value; d rapid deformation, followed by deformation at constant stress, followed by rapid deformation; based on WAWERSIK and BRACE [40]

around  $k_I \approx 0.3 \text{ MN m}^{-3/2}$  in moist air below which no growth seems to occur. In other cases, e.g., liquid water environments, the "threshold" levels are defined operationally as, say, speeds smaller than  $10^{-7} \text{ mm/s}$ , in view of the time required for experiment, but it should be noted that this rate corresponds to approximately 3 mm/yr. and, for long-term earthquake precursory effects, extending over 10 years or so, this is a very rapid speed.

Thus it is of some importance as to whether a true threshold  $k_I$ -level exists and, if so, at what level. Thermodynamics requires that for non-negative entropy production in elastic-brittle crack growth, the "thermodynamic force" associated with crack growth must not be of a different sign than the crack speed  $V$ . This force is the difference between IRWIN's elastic energy release rate and  $2\bar{\gamma}$ , where  $\bar{\gamma}$  is the "surface energy" of a newly exposed crack face as altered by surface adsorption from the environmental species. Thus,

$$\left( \frac{1-\nu}{2G} k_I^2 - 2\bar{\gamma} \right) V \geq 0. \quad (8)$$

For example, the value  $k_I \approx 0.3 \text{ MN m}^{-3/2}$  for glass, if interpreted as a true thermodynamic threshold, would imply a  $\bar{\gamma}$ -value (i.e., that which makes the "force" vanish) of approximately  $0.4 \text{ J/m}^2$ . If long-term surface alterations can reduce  $\bar{\gamma}$  below this value, then the  $k_I$ -level is not a thermodynamic threshold, although obviously the kinetics of any such growth would be extremely slow on a laboratory time scale.

We may note further that thermodynamics does not prohibit a negative value of  $\bar{\gamma}$  in a sufficiently reactive environment. In this case there is no thermodynamic threshold to growth and growth is necessarily irreversible against subsequent healing, in the sense that the entropy production inequality above prohibits a negative  $V$ . But positive  $\bar{\gamma}$ -values allow the thermodynamic possibility of crack healing, and this may be an important mechanism of long-term strength recovery after faulting in lightly shear-stressed rock.

The significance of the moisture effect on crack growth is suggested by Fig. 2b. In compressed rock undergoing a process of local tensile microcracking from the tips of fissures sliding under frictional resistance, the stress intensity  $k_I$  at the microcrack tip can be expected to be approximately proportional to  $\tau - s$  when the tensile crack is very short compared to the sliding portion, where  $\tau$  is the nominal resolved shear stress in the direction of sliding and  $s$  is the average frictional stress that resists sliding. Thus, for very long-time stress alterations in moisture-containing rocks, the required  $\tau - s$  for the onset of microcracking will be proportional to some near-threshold  $k_I$ -value, whereas short-time laboratory tests will show the onset of microcrack growth at the larger  $\tau - s$ -value appropriate to an effective critical  $k_I$ -value for more rapid crack speeds. For the same reason, it may be expected that the entire stress-strain curve in the regime of microcrack growth will be reduced in comparison to short-time laboratory tests, as suggested by Fig. 2c. Note that the stress-strain curves in the non-linear regime, reflecting the initiation and growth of microcracks, are determined by the speeds  $V$  of crack growth at the prevailing crack-tip  $k_I$ -levels. If we simplify the  $V$  vs.  $k_I$  relation to say that a short-time critical  $k_I$ -value applies for rapid crack growth and a smaller long-time critical value for slow crack growth, then the solid and dashed lines in Fig. 2c correspond to continuously meeting conditions for  $k_I$  to be at its short- or long-time "critical" values, respectively.

More generally, such considerations suggest a framework for rock-constitutive relations in which the microcrack network and imposed stresses are regarded as independent variables on which the strain depends, albeit in a manner that suitably incorporates the "path dependence" in stress space that arises from frictional contact. Further, because local stress intensity factors are determined in a similar way by imposed stresses and the existing microcrack network, the rate of enlargement of the network should be expressible in terms of the same two quantities, as a generalization of  $V$  vs.  $k_I$  data as in Fig. 2a. Obviously, to carry out the implied constitutive development it is necessary that suitable "internal variables" be identified to characterize the crack network, and this has not yet been done.

Nevertheless, the concepts are useful for discussing the stress-strain relation of Fig. 2d, based on WAWERSIK and BRACE [40], and involving rapid deformation to  $A$  under rapid stress increase, followed by deformation at constant stresses from  $A$  to  $B$ , followed by rapid deformation beyond  $B$ . Evidently, the deformation from  $A$  to  $B$  results from time-dependent microcrack extension under local  $k_I$ -levels that are, at least at  $B$ , reduced from those appropriate to rapid loading. But the rapid stress increase in the range  $B$  to  $C$  may be assumed to involve little crack growth. Instead, the local stress intensities  $k_I$  are building in size, and when these attain a level consistent with rapid crack growth, e.g., near point  $C$ , the original stress-strain curve appropriate to rapid deformation is rejoined. Thus  $BC$  in Fig. 2d may be interpreted approximately as an iso-crack-network line, corresponding to stress increase with local frictional sliding on fissures but with negligible crack growth. This suggests that hold-time tests of the type described might enable an experimental characterization of the microcrack network in terms of the strain (such as that at  $C$ ), which would correspond to the same (or an approximately equivalent) network in a rapid deformation test.

Such concepts, based on time-dependent crack growth, have not yet been developed into a full enough constitutive description of rock to use in conjunction with the rupture models of Fig. 1 and the subsequent sections. Neither is a full enough experimental background on moisture-assisted crack growth available to examine their relevance for long-time precursory behavior, e.g., on a 10 yr. time scale. Thus there can be little incorporation of the effects in the following analyses, although such considerations, together with the assessment of long-term re-strengthening processes as in the DIETERICH [9] study of fault gouge, would appear to be important themes for future work.

### 3. Instability based on inclusion model

Now, with reference to Fig. 1b and the discussion of Section 2.2.2, consider an inhomogeneous zone which, for simplicity of analysis, is assumed to take the form of an ellipsoidal inclusion in nominally elastic and homogeneous surroundings. As remarked earlier, the stress field within the inclusion is uniform if it is of homogeneous material and the shear-stress mismatch between the inclusion and the far-field is related to the shear-strain mismatch by the ESHELBY relation

$$\gamma_{\text{inc}} - \gamma_{\infty} = (\xi/G) (\tau_{\infty} - \tau_{\text{inc}}). \quad (9)$$

Here the subscript "inc" refers to the inclusion, and the properties which enter ( $G$  and  $\xi$ , given by equations (5) to (7)) are those of the elastic surroundings. Further,  $\gamma_{\infty} = \tau_{\infty}/G$ . This relation for shear is one component of the general ESHELBY relation

$$(\varepsilon_{ij})_{\text{inc}} - (\varepsilon_{ij})_{\infty} = Q_{ijkl} [(\sigma_{kl})_{\infty} - (\sigma_{kl})_{\text{inc}}], \quad (10)$$

where the tensor  $Q_{ijkl}$  is given in specific cases through the work of RUDNICKI [31] and, of course, the  $(\epsilon_{ij})_{\infty}$  are related to the  $(\sigma_{kl})_{\infty}$  by the elastic stress-strain relations of the surroundings.

For simplicity we shall work with equation (9) rather than (10) and assume that  $\tau_{inc}$  is given as a function of  $\gamma_{inc}$  for the inclusion material. First, following RUDNICKI [30], [31], assume that the inclusion represents some "weakened zone" and that its stress-strain relation has the form marked "inclusion" in Fig. 3a. Two comments are in order: First, the inclusion may dilate as it shears and, due to the constraint of the surroundings, additional compressive stresses are induced (we ignore pore fluid effects for the present). These will strengthen the inclusion material and elevate its shear stress-strain curve by comparison to that at constant mean stress. For a given multi-axial stress-strain relation of the inclusion material these effects can be fully estimated (see RUDNICKI [31]); for simplicity here we shall assume that the  $\tau_{inc}$  vs.  $\gamma_{inc}$  relation shown for the inclusion in Fig. 3a represents the in-situ relation, already incorporating any effects of compressive stresses induced by dilation against the constraints of the surroundings. Second, RUDNICKI's [31] comparison of runaway instability conditions for inclusions with the localization bifurcation conditions of RUDNICKI and RICE [32]

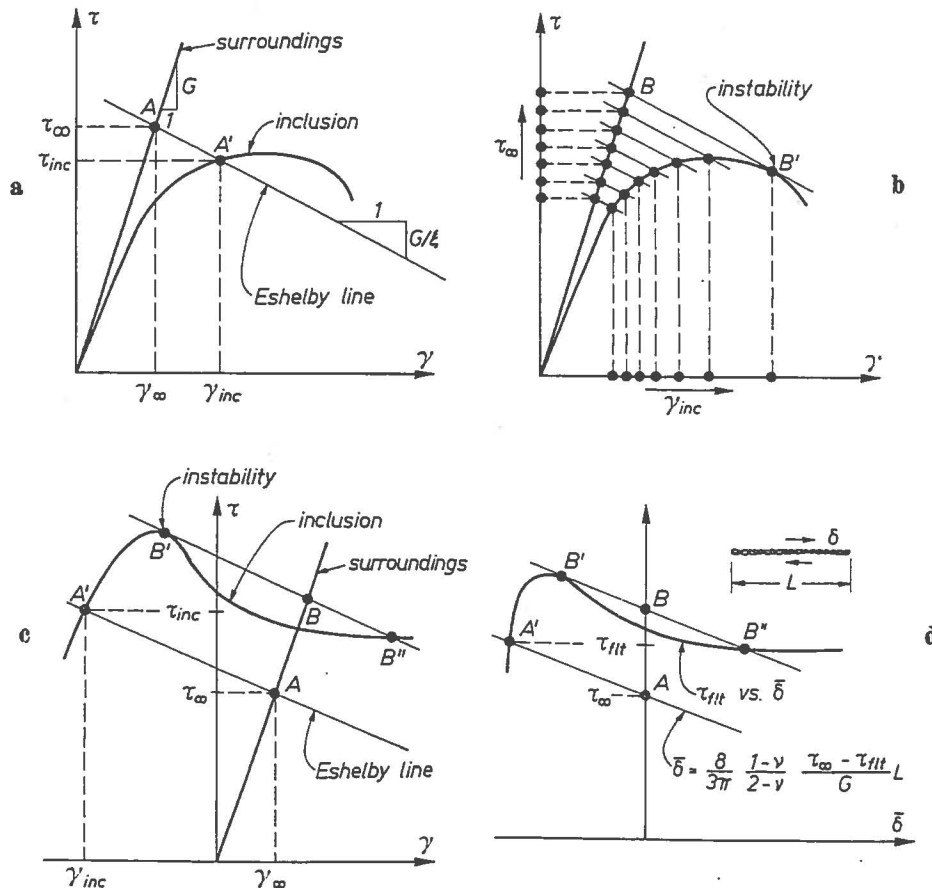


Fig. 3. Deformation and instability of inhomogeneous zones. a Weakened zone; b approach to instability; c seismic gap zone; d fault zone;  $\delta$  is relative slip,  $\tau_{fit}$  is stress

suggests that localization conditions may often be met before runaway. Hence the presumed stress-strain relation for the inclusion may not reflect uniform deformation, but rather deformation that is locally non-uniform and broken-up into incipient small faults. Indeed, later in connection with the discussion of Fig. 3 d, the case of an inhomogeneous zone having, from the start, the form of a shear fault is considered.

Returning to Fig. 3 a, the determination of the state of stress and strain induced within the inclusion by a given remote tectonic stress  $\tau_\infty$  can be reduced to a simple graphical construction as explained by RICE et al. [27]: In addition to the non-linear  $\tau_{\text{inc}}$  vs.  $\gamma_{\text{inc}}$  relation for the inclusion, we draw a straight line representing the linear stress-strain relation,  $\tau_\infty = G\gamma_\infty$ , of the remote surroundings. Now let  $\tau_\infty$  and  $\gamma_\infty$  be chosen to correspond to point  $A$ . The stress and strain differences satisfy the ESHELBY relation, equation (9), so that the state  $\tau_{\text{inc}}, \gamma_{\text{inc}}$  must be a point on the "ESHELBY line" shown, of negative slope  $G/\xi$ , through  $A$ . The state must also lie on the inclusion stress-strain curve, and this defines the point  $A'$  shown, corresponding to  $\tau_{\text{inc}}$  and  $\gamma_{\text{inc}}$ .

If  $\tau_\infty$  is increased by tectonic processes as in Fig. 3 b, the succession of inclusion states is determined by intersection with the succession of ESHELBY lines (all of the same slope). Finally, when  $\tau_\infty$  reaches point  $B$ , the inclusion is at point  $B'$  and no further tectonic stress increase can be sustained. This is an instability point ("run-away"), and the inclusion strains dynamically to some final state. As remarked in the earlier discussion, at this instability point the strain-softening slope of the inclusion has fallen to the "elastic unloading" slope (i.e., slope of ESHELBY line) of the surroundings.

Fig. 3 b has been drawn so that the  $\tau_\infty$ -values shown are equally spaced. Hence, if the tectonic stress rate is constant the time interval between successive  $\tau_\infty$ -values is also constant. It is seen, however, that the successive increments of inclusion strain  $\gamma_{\text{inc}}$  are *not* constant. Rather,  $\gamma_{\text{inc}}$  increases at an ever accelerating, although quasi-static, rate until the instability point is reached and dynamic faulting ensues. As mentioned earlier, this acceleration of local deformation rates over remote tectonic rates is a common precursor of fault models and would, presumably, correspond to a relatively long-term effect by comparison to those effects arising from mechanical interactions with pore fluids.

The seismic gap interpretation of the inclusion model is shown in Fig. 3 c. The strain  $\gamma_{\text{inc}}$  which enters formulae like (9) is, of course, measured relative to the unstressed state of the remote surroundings. Hence, for the seismic gap zone,  $\gamma_{\text{inc}}$  is initially negative since the zone misfits by having lagged behind its surroundings in adjustment to long-term tectonic motions. Accordingly, the  $\tau_{\text{inc}}$  vs.  $\gamma_{\text{inc}}$  relation is shown rising to a peak at the left of the linear stress-strain relation for the remote surroundings in Fig. 3 c. However, the analysis proceeds as before. The ESHELBY line through point  $A$  determines the corresponding state  $A'$  of the inclusion, and we note that in contrast to the "weakened zone" model, now the inclusion carries greater stress than the remote surroundings. Instability occurs when the remote surroundings are at  $B$  and the inclusion at  $B'$  as shown. Further, if dynamic perturbations of the presumed uniform strain state and static stress-strain relation within the inclusion are ignored, it may be assumed that the inclusion reaches a final state after faulting given by  $B''$  in Fig. 3 c.

If the inhomogeneous zone in the model of Fig. 1 b is very flat and fault-like, it may be more appropriate to model it as a mathematically planar fault zone. Then the appropriate constitutive relation is a stress vs. relative slip displacement, rather than stress vs. strain, relation. Such relations could be developed by suitable extension of the studies of BARTON [3] and DIETERICH [10]. Now the ESHELBY relation of (9) is replaced by the relation between the relative slip displacement  $\delta$  (i.e., of one side of the fault relative to the other) and the difference between the remote shear stress  $\tau_\infty$  and the shear stress  $\tau_{flt}$  actually carried by the fault. Presuming the latter to be uniform, we have

$$\delta = \frac{4(1-\nu)}{\pi(2-\nu)} L \frac{\tau_\infty - \tau_{flt}}{G} \left[ 1 - \frac{r^2}{(L/2)^2} \right]^{1/2} \quad (11)$$

for the relative displacement at distance  $r$  from the center of a penny-shaped shear fault of diameter  $L$ . For the corresponding plane-strain geometry of a fault of length  $L$  loaded in shear, the above formula applies with

$$\frac{4(1-\nu)}{\pi(2-\nu)} \text{ replaced by } (1-\nu).$$

Recognizing that the displacement on the fault is non-uniformly distributed, for simplicity we shall deal with the area-average fault displacement which is

$$\bar{\delta} = \frac{8(1-\nu)}{3\pi(2-\nu)} L \frac{\tau_\infty - \tau_{flt}}{G} \quad (12)$$

for the penny-shaped geometry, and

$$\bar{\delta} = \frac{\pi(1-\nu)}{4} L \frac{\tau_\infty - \tau_{flt}}{G} \quad (13)$$

for plane strain.

The solid line in Fig. 3 d represents the  $\tau_{flt}$  vs.  $\bar{\delta}$  relation and is drawn to conform in general to BARTON's [3] stress vs. slip observations on "model" faults. The curve is located in the negative  $\bar{\delta}$ -range as appropriate to a seismic gap interpretation. Assuming a penny-shaped geometry, equation (12) gives the line analogous to the ESHELBY line of earlier figures, and it is seen on Fig. 3 d how this allows computation of the fault state at  $A'$  given the remotely applied stress at  $A$ . Instability occurs at points  $B, B'$ .

We note that the unloading stiffness of the surroundings is inversely proportional to the length  $L$  of the fault zone in this interpretation. Also, the fault is being modelled as if it displaces in a more or less uniform way. If instead the mode of motion is the crack-like spread of the slipping region as in Fig. 1 c, then a different analysis is required as in Chapter 4.

Following RUDNICKI [30] and RICE et al. [27], we now examine the means discussed in Section 2.3 by which mechanical interactions between the host rock and pore fluids might lend initial stability to the inhomogeneous zones considered, in the sense that abrupt failure does not occur at points  $B'$  in Fig. 3. Rather, an initially quasi-static period of accelerating strain then begins, on a time scale controlled by fluid transport, and this leads finally to the dynamic instability.

### 3.1. Dilatant hardening of inhomogeneous zone

Consider an element of material that is stressed by a combination of pure shear  $\tau$ , hydrostatic compression  $\sigma$ , and pore pressure  $p$ . First we consider drained deformations (i.e., for  $p$  constant). When the stresses are altered so as to cause elastic response, without frictional slip or microcracking, it is supposed that the incremental shear and dilatant strains are

$$d\gamma = d\tau/G, \quad d\varepsilon = -d\sigma/K, \quad (14)$$

where  $G$  and  $K$  are elastic shear and (drained) bulk moduli; with reference to the inclusion model, these are not necessarily to be identified with corresponding moduli in the surroundings. For more general stress increments we append "plastic" portions  $d^p\gamma$ ,  $d^p\varepsilon$  to the above expressions in the manner of RICE [24] and RUDNICKI and RICE [32], assuming like them that a dilatancy factor  $\beta$  relates the non-elastic dilation to the non-elastic shear,

$$d^p\varepsilon = \beta d^p\gamma, \quad (15)$$

since both have their origin in frictional slipping and opening of microcracks. Further, they assume that for stress increments causing non-elastic response

$$d^p\gamma = (d\tau - \mu d\sigma)/h, \quad (16)$$

where  $h$  is the inelastic hardening (or softening, if negative) modulus and  $\mu$  a frictional coefficient. RUDNICKI and RICE [32] suggest that for rocks studied by BRACE et al. [7] and others, representative ranges of  $\beta$  and  $\mu$  are 0.2 to 0.6 and 0.5 to 1.0, respectively.

If alterations in the pressure of the infiltrating pore fluid are now considered in the manner of RICE [24], for the elastic part of the deformation we replace

$$d\sigma \quad \text{with} \quad [d\sigma - (1 - K/K_s) dp],$$

where  $K_s$  is the bulk modulus of the solid phase (e.g., see RICE and CLEARY [26]), and for the "plastic" part of the deformation we replace

$$d\sigma \quad \text{with} \quad (d\sigma - dp).$$

Then the complete incremental constitutive relations, assuming inelastic response, are

$$d\gamma = \frac{d\tau}{G} + \frac{d\tau - \mu(d\sigma - dp)}{h}, \quad (17)$$

$$d\varepsilon = -\frac{d\sigma - dp}{K} - \frac{dp}{K_s} + \beta \frac{d\tau - \mu(d\sigma - dp)}{h}. \quad (18)$$

To these we must add a relation for the increment  $dm$  of fluid mass  $m$  per unit volume. This is given in terms of the void-(or pore-)space volume fraction  $v$  by  $m = \rho v$ , where  $\rho = \rho(p)$  is the mass density of the fluid. Using the reciprocity relations discussed by RICE [24] and RICE and CLEARY [26] for the elastic portion of  $dv$  and assuming that the non-elastic portion is equal to  $d^p\varepsilon$  (RICE [24]), one may write

$$\frac{1}{\rho} dm = \frac{v dp}{K_f} - \left[ \frac{1}{K} - \frac{1}{K_s} \right] (d\sigma - dp) - \frac{v}{K_s} dp + \beta \frac{d\tau - \mu(d\sigma - dp)}{h}, \quad (19)$$

where  $K_f$  is the bulk modulus of the fluid.

We may now compare the stiffness of response in shear for drained and undrained conditions. In particular, considering deformation at constant hydrostatic stress,  $d\sigma = 0$ , one computes a strain-hardening slope in shear under drained conditions by setting  $dp = 0$  in (17), giving

$$\left(\frac{d\tau}{d\gamma}\right)_{\text{drained}} = \frac{h}{1 + h/G}, \quad (20)$$

so that the total shear stiffness is essentially equal to the "plastic" modulus  $h$  of (16) when this is small compared to  $G$ . By contrast, for undrained conditions one sets  $dm = 0$  in (19) so that pore fluid alterations

$$dp = -\frac{\beta K'}{h + \mu\beta K'} d\tau \quad (21)$$

occur as shear commences and, by (17), the corresponding strain-hardening slope is

$$\left(\frac{d\tau}{d\gamma}\right)_{\text{undrained}} = \frac{h + \mu\beta K'}{1 + (h + \mu\beta K')/G}, \quad (22)$$

where the modulus  $K'$  is given by

$$\frac{1}{K'} = \frac{1}{K} + \frac{v}{K_f} - \frac{1+v}{K_s}. \quad (23)$$

In comparing (20) and (22), it is seen that for undrained conditions the material deforms as if its plastic hardening modulus were  $h + \mu\beta K'$  rather than  $h$ . Given the representative sizes of  $\beta$  and  $\mu$  and since, by (23),  $K'$  will be of the same order as the smallest of the drained bulk modulus  $K$  and the quantity  $K_f/v$ , this is an important effect. Indeed, it is possible that  $h$  would be negative while  $h + \mu\beta K'$  is positive, so that the material softens if drained and hardens if undrained. For heavily fissured rock, the last term in (23) can be ignored and

$$K' \approx \frac{KK_f}{K_f + vK}. \quad (24)$$

For liquid water at temperatures well below the critical point,  $K_f$  ( $\approx 33$  kbar) is on the order of  $K_s/10$  ( $> K/10$ ) and, for most rocks,  $v$  is much less than  $1/10$ , so that the term  $vK$  in (14) is negligible and  $K' \approx K$ . On the other hand, if  $K_f$  is reduced to values much smaller than  $vK$  by high temperature, low pore pressure, or the incomplete saturation of pore space (e.g., if the "pore fluid" is liquid with entrapped gas bubbles), then  $K' \approx K_f/v$  and, of course,  $K'$  vanishes with  $K_f$ , the dilatant hardening effect disappearing in that limit.

The application of these results to the inclusion model is not simple for two reasons. First, the constraints of the surroundings must be taken into account. As remarked earlier, the  $\tau_{\text{inc}}$  vs.  $\gamma_{\text{inc}}$  curves of Fig. 3 are intended to be in-situ relations, including the effects of dilatantly induced compressive stresses. Thus the in-situ values of  $(d\tau/d\gamma)$  will not be as given by (20) and (22), although the undrained in-situ slope is steeper than the drained and can, e.g., likewise be positive when the drained slope is negative. Second, the response of the inhomogeneous zone is, of course, not fully undrained. Instead, a diffusion process is established by which the induced suctions are gradually alleviated. This requires for its full analysis that ESHELBY relations such as

(9), (10) be replaced by a more general set of time-dependent relations between the values of  $\sigma_{ij}$ ,  $p$ ,  $\varepsilon_{ij}$ , and  $m$  within and outside the inclusion. Such relations have been derived by RICE et al. [27] for the special case of a spherical inclusion that is assumed to be highly permeable, by comparison to its surroundings, so that the pore pressure can be taken as essentially uniform (although time-dependent) within it.

The reader is referred to RUDNICKI [30] for the beginning of an analysis of the coupled dilatant hardening processes that take place beyond the "instability" point  $B'$  (as predicted on the assumption of fully drained response) in Fig. 3. In fact, RUDNICKI neglects the time dependence of elastic stiffness of the inclusion surroundings in his analysis, and concentrates instead just on the stabilization that arises from dilatant hardening. The same is done here in the discussion of the following two paragraphs, and the complementary stabilization, arising from time-dependent elastic stiffness, is taken up in the next section.

Indeed, with reference to Fig. 4, if there is only a small change in  $\tau_\infty$  from its value at the instability point, according to the drained analysis, the dilatant hardening effects will cause the inclusion state to move parallel to the ESHELBY line through  $B'$ , deviating from the dashed line continuation of the inclusion stress-strain curve for fully drained conditions. The system is not dynamically unstable at  $B'$  because, for rapid deformations, the slope  $(d\tau/d\gamma)$  has its undrained value, corresponding to the direction of the arrow marked  $u$  emanating from  $B'$ . Of course, the corresponding arrow  $d$  for drained conditions has the direction of the ESHELBY line at  $B'$ . As the system deforms, on a time scale controlled by fluid diffusion, continued softening causes both the  $u$ - and  $d$ -values of  $(d\tau/d\gamma)$  to diminish, e.g., point  $C'$  in the figure. Finally, a point  $D'$  is reached at which the undrained  $(d\tau/d\gamma)$  has fallen in value to that of the elastic unloading slope, and dynamic instability occurs.

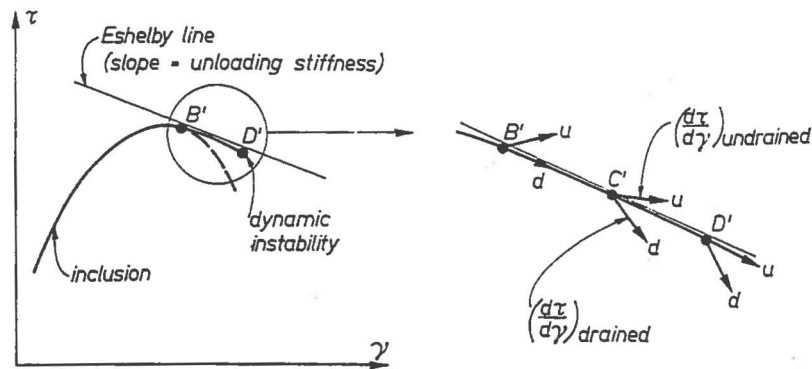


Fig. 4. Stabilization of inhomogeneous zone by dilatant hardening; dynamic instability delayed to  $D'$

While the full details of the process have not yet been worked out, e.g., for the prediction of the rapid-creep-strain precursory time interval between  $B'$  and  $D'$ , it seems evident that the process as described would involve a continuous regional lowering of pore pressure up to the dynamic instability, without a period of pressure recovery as imagined in some interpretations of  $V_p/V_s$ -anomalies. On the other hand, the model envisions more or less homogeneous strain within the inclusion up to the dynamic instability, and it is possible that some gradual localization process could alter the above conclusion.

### 3.2. Time-dependent stiffness of surroundings

As remarked previously and, more extensively, in Section 2.3.2, a second source of stabilization arises because the surroundings, when fluid-infiltrated, respond in an elastically stiffer fashion to short-time stress alterations than to long-time. This effect will always occur in combination with the dilatant hardening effect and, at least for the inclusion model, it might be expected that both would have approximately comparable time scales.

However, for simplicity of discussion we now assume that no dilatancy occurs within the inclusion, its response being considered to be the same as if fully drained, and we consider the inclusion when it has reached the point  $B'$  in Fig. 5. The solid ESHELBY line represents the elastic unloading stiffness of the surroundings, assuming drained elastic properties, but dynamic instability does not occur at  $B'$  because the *undrained* elastic unloading stiffness, indicated by the dashed line, governs short-time stress alterations. Representative stiffness differences that are expected for different crack densities are shown in the last three columns of Table 1. For clarity of illustration, the figure has been drawn with a much greater stiffness difference than any listed in the table.

Because of these effects, the system continues to deform along the inclusion stress-strain curve, again on a time scale controlled by fluid diffusion and the inelastic stress-strain relation that is being followed. Finally the system reaches the point  $D'$  at which the softening slope equals the *undrained* elastic unloading stiffness and dynamic instability occurs.

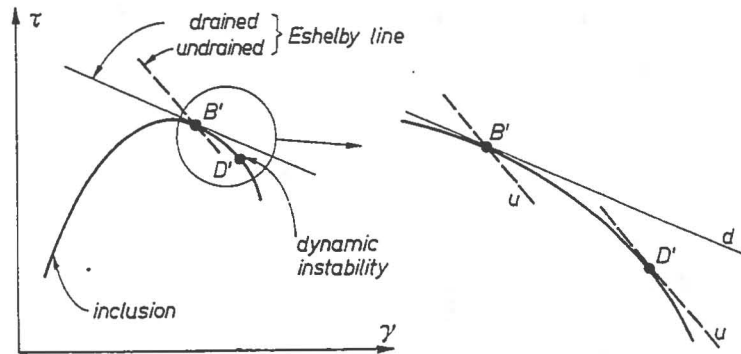


Fig. 5. Stabilization due to time-dependent elastic stiffness. The solid straight line represents the unloading stiffness for drained ( $d$ ) conditions, the dashed line for undrained ( $u$ ) conditions. Actual stiffness changes,  $d$  to  $u$ , will be smaller than shown

For a fuller analysis of the process one must employ the time-dependent generalization of the ESHELBY relations for fluid-infiltrated solids as discussed earlier. Indeed, for a highly permeable spherical inclusion deforming under pure shear loading, RICE et al. [27] found that the time-dependent strain state within the inclusion continues to be spatially uniform (it is not known at present if this result applies to any wider class of inclusions). Further, equation (9) then generalizes to

$$\gamma_{\text{inc}}(t) - \gamma_{\infty}(t) = 1/G \int_{-\infty}^t \{ \xi_u + (\xi - \xi_u) f[c(t-t')/a^2] \} [\dot{\tau}_{\infty}(t') - \dot{\tau}_{\text{inc}}(t')] dt', \quad (25)$$

where  $t$  is time, the superposed dots denote time rates,  $\xi$  and  $\xi_u$  are given by (7) with  $v_e$  equal to  $v$  (drained) and  $v_u$  (undrained) respectively,  $a$  is radius of the inclusion,  $c$  is the diffusivity of the pore fluid as it appears in the BIOT consolidation equations, and  $f[. . .]$  is a certain dimensionless function.

In fact,  $f(\theta)$  with  $\theta = ct/a^2$  arises in the solution for the "strain"  $\gamma$  of the interior of a spherical cavity, with wall maintained at zero pore pressure, when the remote surroundings of the cavity are subjected to a step-function increase in shear stress  $\tau_\infty$  at  $t = 0$ . The function is plotted in Fig. 6, taken from RICE et al. [27] with their parameter  $\eta$  (on which  $f(\theta)$  depends in only a very weak fashion over its admissible range) set equal to 0.8. The figure also shows the relation of  $f(\theta)$  to the cavity "strain"  $\gamma$ , which varies from its instantaneous undrained value  $\gamma_u$ , at  $\theta = 0+$ , to its fully drained value  $\gamma_d$  as  $\theta \rightarrow \infty$ . The other curve in Fig. 6 will be explained shortly.

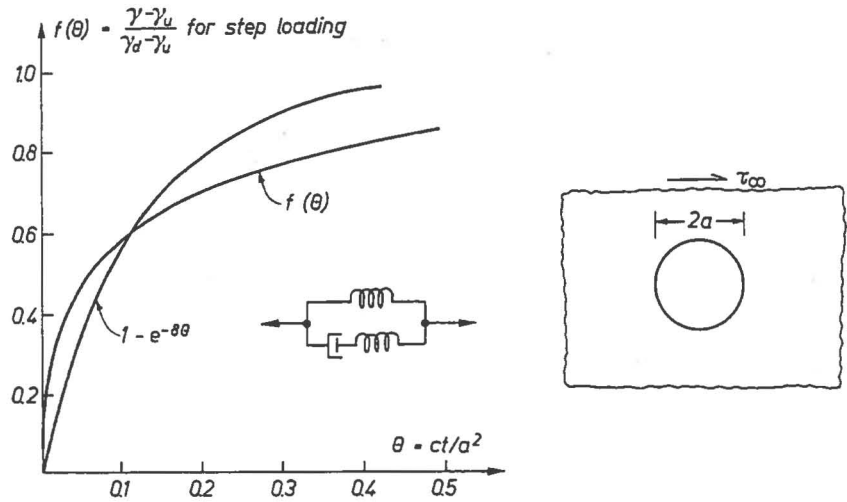


Fig. 6. Function  $f(\theta)$  arising in response of spherical cavity to step-shear loading, from RICE et al. [27] with  $\eta = 0.8$ ; approximation based on standard linear model also shown

It is to be realized that (25) is, in effect, an integral equation for the strain within the inclusion. The given quantity is the tectonic stress  $\tau_\infty(t)$  (note that  $\gamma_\infty = \tau_\infty/G$ ), and the stress  $\tau_{inc}$  within the inclusion is considered to be a function of  $\gamma_{inc}$  as in Fig. 5, for example. Thus (25) enables one, in principle, to solve for  $\gamma_{inc}$ , at least up to the dynamic instability point  $D'$  in Fig. 5. The details of doing so have not yet been carried out. The following section outlines a *very* approximate estimate of the precursory time interval involved in the diffusion-controlled creep instability process from  $B'$  to  $D'$  in Fig. 5. It is to be understood as being suggestive only, and not definitely indicative of the results of a more precise analysis.

### 3.2.1. Approximate estimate of precursor time

First, as suggested by the second curve in Fig. 6 we approximate the response of the spherical zone to step loading by that of a "standard linear model". The fit is far from perfect, the best match being made with a "relaxation time" of  $1/8$  in dimensionless time  $\theta$ , or in terms of real time

$$t_r \approx a^2/8c \approx 0.1 a^2c, \tag{26}$$

as shown. The equation analogous to the integral relation of (25) can then be written in differential form as

$$\left(t_r \frac{d}{dt} + 1\right) (\gamma_{inc} - \gamma_\infty) = \frac{1}{G} \left(\xi_u t_r \frac{d}{dt} + \xi\right) (\tau_\infty - \tau_{inc}). \quad (27)$$

Here the parameters of the standard linear model are chosen to give correct short- and long-term limits. Next, with reference to Fig. 7, the inclusion stress-strain curve in the vicinity of peak strength and beyond is represented in the form

$$\tau_{inc} = \tau_p - \frac{G}{2\lambda} (\gamma_{inc} - \gamma_p)^2. \quad (28)$$

Here,  $\tau_p, \gamma_p$  are the peak stress and strain and, as shown, the curve is a parabola which joins with continuous slope onto a straight line portion at a strain  $\lambda$  prior to peak.

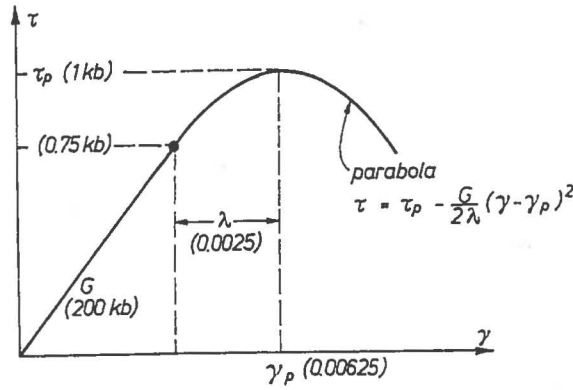


Fig. 7. Inclusion stress-strain relation for analysis of time-dependent elastic stiffness effects on stabilization of rupture

Inserting this into (27) and assuming that the tectonic stress rate  $\dot{\tau}_\infty$  is constant, (27) becomes the differential equation

$$t_r \frac{dz}{dt} = \frac{(\zeta + \alpha t/t_r) Q - z(1 - \alpha z/2)}{1 - z}, \quad (29)$$

where  $t = 0$  when  $\gamma_{inc} = \gamma_p$ , and where

$$z = \xi_u (\gamma_{inc} - \gamma_p) / \lambda, \quad \alpha = \xi / \xi_u, \quad Q = \xi(1 + \xi) t_r \dot{\tau}_\infty / (G \lambda \alpha^2)$$

and

$$\zeta = \frac{\alpha + \xi}{1 + \xi} + \alpha \frac{(\Delta\tau_\infty)_0}{t_r \dot{\tau}_\infty}, \quad (30)$$

with  $(\Delta\tau_\infty)_0$  being the difference between the actual value of  $\tau_\infty$  and that which would correspond to equilibrium under fully drained conditions at  $\gamma_{inc} = \gamma_p$ .

Note that  $z = 0$  initially and that the dynamic instability point  $D'$  of Fig. 5 corresponds to  $z = 1$ . Also,  $\alpha$  is the undrained to drained stiffness ratio for which values are shown in Table 1. The parameter  $Q$  expressing the tectonic loading rate will, in general, be very small by comparison to unity.

Equation (29) has been solved numerically by writing this as an equation for  $d(t/t_r)/dz$ , and a precursory time interval  $t_{prec}$  is defined as the time for  $z$  to go from 0 to

Table 2. Dimensionless precursor time for transition from drained to undrained instability point ( $B'$  to  $D'$  in Fig. 5), in terms of dimensionless tectonic stress rate  $Q$  of equation (30), for stiffness ratio of 1.25

$Q$	$1.3 \times 10^{-4}$	$3.2 \times 10^{-4}$	$1.3 \times 10^{-3}$	$3.2 \times 10^{-3}$	$1.3 \times 10^{-2}$	$3.2 \times 10^{-2}$
$t_{\text{prec}}/t_r$	6.0	3.9	1.9	1.1	0.5	0.3

1, corresponding to the self-driven creep process from  $B'$  to  $D'$  in Fig. 5. Calculations become expensive for small  $Q$ , because the step size must be decreased proportionally. Table 2 shows results based on  $\alpha = 1.25$  (which, judging from Table 1, probably overestimates the effect somewhat) and  $\xi = 1.125$ . The latter would correspond to  $(\Delta\tau_\infty)_0 = 0$  and  $\xi = 1$ , which is reasonable for a spherical zone.

The results of the table can be better appreciated in a dimensional form. To do this we choose  $G$  and  $\lambda$  as in Fig. 7 (none of the other parameters of the figures are relevant to the prediction of  $t_{\text{prec}}$ ), we choose  $\dot{\tau}_\infty$  as 1 bar/yr., we consider two values of  $a$ , namely 1 km and 5 km, and we examine results for  $\xi = 1$  and 10. The first of these is reasonable for a sphere; the second approximates to a flattened axi-symmetric ellipsoid with aspect ratio of a little less than 20, equation (6), and we regard  $a$  as its semi-major axis and refer to it as a "slit". Further, we examine two values of the diffusivity  $c$ , namely 1 m<sup>2</sup>/s, which is a value suggested by ANDERSON and WHITCOMB [1] as being reasonable for shallow earthquake regions, and a smaller value 0.1 m<sup>2</sup>/s, which is more nearly in accord with well-head measurements near the San Andreas fault (KOVACH et al. [14]). The results are shown in Table 3, where, for each value of  $a$  and  $c$ , the precursory time  $t_{\text{prec}}$  is given for a "sphere" ( $\xi = 1$ ) and "slit" ( $\xi = 10$ ). The diffusive relaxation time  $t_r$  of (26) is shown as well. Note that the results for spheres of the 1 km radius require smaller values of  $Q$  than those of Table 2, and the results shown were estimated by extrapolation on a semi-log plot of  $Q$  against  $t_{\text{prec}}/t_r$ .

Table 3. Predicted precursory periods in days [d] for the accelerated creep process taking place after achievement of instability conditions based on drained elastic properties of surroundings; based on ratio of undrained to drained elastic unloading stiffness of 1.25; last column: based on a best-fit line of SCHOLZ et al. [34] through precursory data from  $V_p/V_s$ -anomalies, radon emissions, and crustal movements, with  $2a$  identified as the length of the aftershock zone

	$c = 1 \text{ m}^2/\text{s}$	$c = 0.1 \text{ m}^2/\text{s}$	SCHOLZ et al. [34]
$a = 1 \text{ km}$	$t_r = 1.2 \text{ d}$ $t_{\text{prec}} = \begin{cases} 4 \text{ d, slit} \\ 23 \text{ d, sphere} \end{cases}$	$t_r = 11.6 \text{ d}$ $t_{\text{prec}} = \begin{cases} 12 \text{ d, slit} \\ 120 \text{ d, sphere} \end{cases}$	$t_{\text{prec}} \approx 8 \text{ d}$
$a = 5 \text{ km}$	$t_r = 29 \text{ d}$ $t_{\text{prec}} = \begin{cases} 17 \text{ d, slit} \\ 145 \text{ d, sphere} \end{cases}$	$t_r = 290 \text{ d}$ $t_{\text{prec}} = \begin{cases} 38 \text{ d, slit} \\ 435 \text{ d, sphere} \end{cases}$	$t_{\text{prec}} \approx 200 \text{ d}$

The last column of the table is based on a "best-fit" correlation by SCHOLZ et al. [34] of precursory time intervals (based on  $V_p/V_s$ -anomalies, radon emission, and crustal movement) with length of the aftershock zone, identified here as  $2a$ . Of course, the actual events on which the line is based deviate by factors of the order of 2 or so from this line. The predicted results correspond well enough with the range of the data that it would seem advisable to give a fuller examination to the role of pore fluids in stabilizing earthquake ruptures.

4. Spread of slipping region on fault

In this chapter we consider models for the inception of rupture of the type in Fig. 1 c, in which a slipping region spreads in a shear-crack mode under initially quasi-static conditions until instability conditions, marked by dynamic, inertia-limited fault propagation, are met. Some aspects of this type of model have been discussed in Section 2.2.3 and, as emphasized there, predictions of whether the slipping region spreads in a stable quasi-static, or in an unstable dynamic, manner are sensitive to heterogeneities of strength and driving stress and also, of course, to details of the constitutive dependence of the local shear stress,  $\tau$ , along the fault on the relative slip,  $\delta$ . As remarked earlier, work such as that of BARTON [2], [3], DIETERICH [9], [10] and others reveal dependences of  $\tau$  on  $\delta$  at the onset of slip, on  $\delta$  during steady slip, on the time of stationary contact, on the relative roughness of the sliding surfaces and strength of the adjacent rock, possibly as influenced by surface-chemical effects of pore fluids, and, of course, on the intensity of the effective normal stress,  $\sigma - p$ .

A constitutive description inclusive of rate effects due, e.g., to chemical factors and bonding at micro-contacts seems out of reach at present, but some principal features of constitutive response at the onset of relative slippage on a well-bonded, previously quiescent fault can be included with reference to Fig. 8. This is based on the slip-surface model of PALMER and RICE [22]; see also RICE [23] and RICE and CLEARY [26]. The upper portion of the figure shows the edge of a slipping region which is spreading along a fault, and the distribution of shear stress  $\tau$  is considered to be such that a critical level  $\tau_B$  is needed to initiate the "breakdown" process at the fault tip, and that  $\tau$  falls gradually to a limiting friction level  $\tau_F$  within a "breakdown zone" of size  $\omega$ . In fact, as shown on the lower left, the stress  $\tau$  is taken as some softening function of the relative slip, and (lower right) the levels  $\tau_B$  and  $\tau_F$ , as well as the entire  $\tau$  vs.  $\delta$  function, are elevated by increases in the effective normal stress,  $\sigma - p$ .

PALMER and RICE [22] showed that the cross-hatched area may be identified as the critical fracture mechanics energy release rate,  $\mathcal{G}_{crit}$ , for fault spreading. This arises in the sense that the spreading criterion predicted by their model may be cast in the

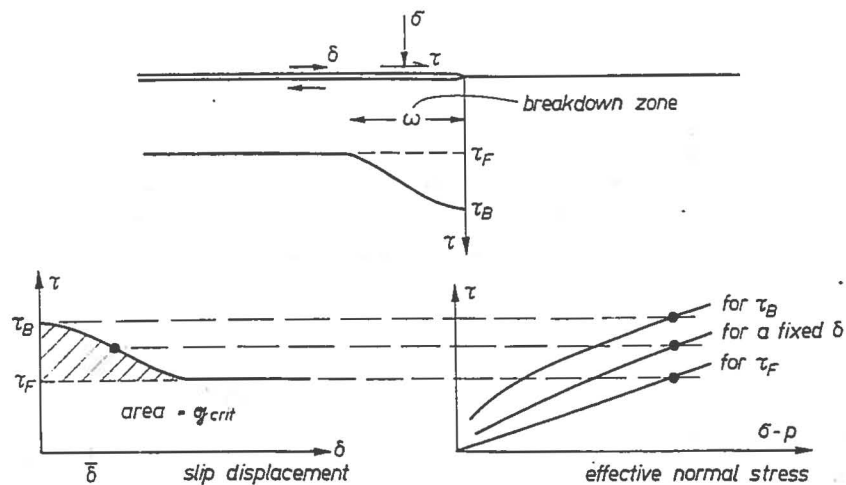


Fig. 8. Processes near the edge of a slipping region which is spreading along a fault. The strength  $\tau$  depends on relative slip  $\delta$  and effective stress  $\sigma - p$ , and although not shown, on slip rate  $\dot{\delta}$  and time of stationary contact. After RICE and CLEARY [26]

elastic fracture mechanics form of equation (1) whenever the breakdown zone size  $\omega$  is small compared to overall dimensions of the slipping region, where  $k$ , for which the critical value is given by (1), is the shear-mode elastic stress intensity factor that would be calculated if the breakdown zone were ignored and the stress on the fault assumed to equal  $\tau_F$  everywhere. This  $k$  is proportional to the excess of  $\tau_\infty$  over  $\tau_F$ . For example, if the slipping region in Fig. 1c has a penny-shaped form of diameter  $L$ , then

$$k = \frac{4}{(2 - \nu)\pi} (\tau_\infty - \tau_F) (\pi L/2)^{1/2} \quad (31)$$

at the edges which advance by in-plane shear (anti-plane shear conditions prevail at the edges  $90^\circ$  removed from these, and mixed shear at all other locations; these necessitate appropriate but well-known generalizations of (1)). Also, for the corresponding plane-strain shear-fault model,

$$k = (\tau_\infty - \tau_F) (\pi L/2)^{1/2} . \quad (32)$$

The parameter  $\bar{\delta}$  indicated on Fig. 8 is a measure of a representative slip displacement for the breakdown process, and it is defined by

$$\bar{\delta} = (\text{Area})/(\tau_B - \tau_F) = \mathfrak{G}_{\text{crit}}/(\tau_B - \tau_F) . \quad (33)$$

DIETERICH's [10] study of slippage on flat-ground surfaces of Westerly granite suggests a  $\bar{\delta}$ -value of 2 to 3  $\mu\text{m}$ , but it would perhaps be expected that larger-scale roughness protrusions on natural faults would lead to larger  $\bar{\delta}$ -values corresponding, in BARTON's [3] analysis of shear strength, to the slip required to deform or rupture the protrusions. Indeed, results of COULSON, quoted by BARTON ([2], Fig. 6), on shear of a "natural joint in coarse grained granite" suggest  $\bar{\delta}$ -values a thousand times larger, in the range of 2 to 3 mm. The size  $\omega$  of the breakdown zone (Fig. 8) will be much greater than  $\bar{\delta}$  due to the elastic constraint of the surroundings. Using the calculation of PALMER and RICE, based on an assumed linear variation of stress from  $\tau_B$  to  $\tau_F$  over the distance  $\omega$  in the upper diagram of Fig. 8,

$$\omega = \frac{9\pi}{16(1 - \nu)} \frac{G}{\tau_B - \tau_F} \bar{\delta} . \quad (34)$$

For example, taking  $G = 200 \text{ kb}$  and  $\tau_B - \tau_F = 100 \text{ b}$  as representative,  $\omega \approx 12 \text{ m}$  when  $\bar{\delta}$  is 2.5 mm, representative of COULSON's natural joints, and  $\omega \approx 12 \text{ mm}$  when  $\bar{\delta}$  is 2.5  $\mu\text{m}$ , representative of DIETERICH's flat-ground surfaces. Such estimates are important to attempts at laboratory study of confined slipping zones on faults as in Fig. 1c (e.g., DIETERICH [10]);  $\omega$  must be very small by comparison to specimen dimensions for such a region to exist of reasonable similarity to what is, presumably, possible in-situ.

Now, there is ample evidence that the creep-like spread of slipping regions can occur along faults (e.g., KING et al. [13]; NASON and WEERTMAN [19]) and accelerating creep is widely regarded as a typical short-term precursor to earthquakes. Hence it is important to establish the mechanism of creep motions and the conditions under which these destabilize to seismic rupture. As remarked earlier in discussion of STUART's [36] model, some degree of accelerating precursory fault creep seems to be an inevitable prediction, even for a completely rate-independent material model, when spatial heterogeneity of strength along fault surfaces and the gradual build-up of re-

mote tectonic loadings are considered. The reasons are similar to those illustrated for the inclusion model in Fig. 3b. But the creep observations suggest that the process may have a far more rapid time scale and that some essentially rate-dependent aspect of material behavior serves to stabilize the slipping region, in the sense that an increasing stress intensity  $k$  is required for an increasing, but still quasi-static, fault spreading speed  $V$ . This stabilizing mechanism is, presumably, what allows fully stable creep-like slip events as reported by KING et al. [13] to occur. Further, the exhaustion of the stabilizing mechanism corresponds to the transition from precursory fault creep to an earthquake.

Two promising mechanisms for this type of fault stabilization arise from the mechanical interactions with pore fluids in a fluid-infiltrated rock mass, and are described in the next sections. Equally or more important mechanisms might arise from time effects of a surface-chemical type, e.g., from the environmentally assisted growth of micro-cracks in regions of asperity protrusions or from time dependence of gouge cementation at microscopic contacts. Indeed, studies of the friction process like that of DIETERICH [10] may lead to a mechanism based on such considerations, although, to the writer's knowledge, no viable model has yet been proposed.

#### 4.1. Dilatancy in the breakdown region

BARTON [2], [3] emphasizes that natural rock joints brought into stationary contact dilate slightly as they are sheared toward peak strength. Indeed, BARTON further suggests that this dilation can be suppressed only by normal stresses (or, for fully closed joints, combinations of triaxial stresses) that reach levels appropriate to rupture of the rock bordering the joint, and that the transition between sliding with a strength drop, e.g., as in Fig. 8, and fully stable sliding without strength decrease can be explained in terms of attaining stress levels that suppress dilation.

With this in mind we consider in Fig. 9a a model similar to that of RICE [23] for slip surfaces in soils. Here a dilatant opening of total amount  $H$  is assumed to occur within the breakdown zone as the slipping region spreads at a steady speed  $V$  along the fault surface. This dilation induces a suction distribution in the pore fluid, and the particular distribution shown was calculated by RICE [23] in a manner discussed also for the present context by RICE and CLEARY [26], based on the following assumptions: The dilation is assumed to be equivalent to the induction of a flow of liquid into the zone  $\omega$  at a uniform rate, such that a net volume  $H$  per unit area is indrawn in the time  $\omega/V$  that it takes the breakdown zone to pass by. Hence the volumetric flow rate into the fault from each side is  $VH/2\omega$  per unit area (transport along the fault is neglected). The pore pressure field is assumed to satisfy the one-dimensional consolidation equation

$$c\partial^2 p/\partial y^2 = \partial p/\partial t, \quad (35)$$

where  $c$  is the diffusivity and  $y$  the direction normal to the crack. Further, the volumetric flow rate per unit area is  $\kappa \partial p/\partial y$ , where  $\kappa$  is a permeability coefficient, and the diffusion equation is solved subject to the boundary condition that the flow rate at the fault surface be  $VH/2\omega$  while a point is within the breakdown zone, and zero otherwise. The resulting suction ( $-\Delta p$ ) rises in proportion to  $r^{1/2}$ , where,  $r$  is the distance from the tip of the slipping region, and reaches a maximum of (RICE [23]; also RICE and

CLEARY [26], eq. (54))

$$(-\Delta p)_{\max} = H \frac{c}{\kappa} \left( \frac{V}{\pi c \omega} \right)^{1/2} = HM \left( \frac{V}{\pi c \omega} \right)^{1/2} \quad (36)$$

at the trailing edge of the breakdown zone. Here the ratio  $c/\kappa$ , which is independent of fluid transport properties, is written as  $M$ ; this is a kind of elastic modulus (e.g., RICE and CLEARY [26], eq. (17)) and, in the special case for which the fluid and solid constituents are regarded as separately incompressible,  $M$  is the elastic modulus for fully drained one-dimensional straining.

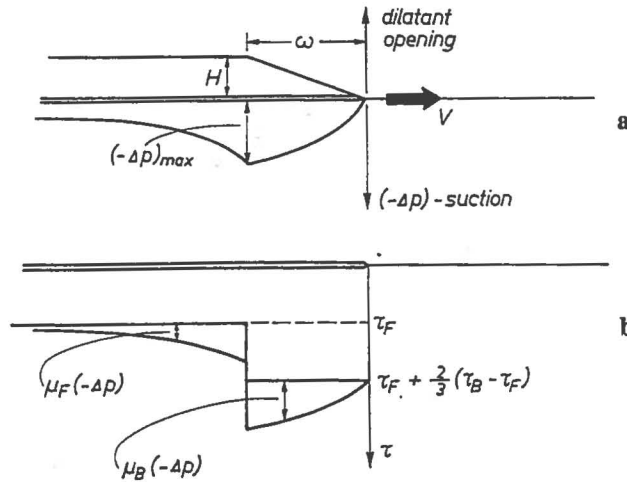


Fig. 9. Dilatancy in fault-tip breakdown zone. **a** Suctions induced by dilatant opening  $H$  as slipping region spreads quasi-statically at speed  $V$ ; **b** shear-stress distribution assumed for analysis of fault stabilization by dilatancy, following RICE [23]; the friction coefficient is  $\mu_B$  in the breakdown zone and  $\mu_F$  along regions of the fault subjected to larger amounts of sliding

The effect of the pressure distribution on the resistance to slip is illustrated in Fig. 9b. Following RICE [23], the basic frictional resistance, without pore-pressure effects, is simplified to piece-wise constant stress distribution shown, with the drop from one level to the other at  $\delta = 3\bar{\delta}/2$ . The  $2/3$ -factor on stress and  $3/2$  on displacement are chosen so that the area under the  $\tau$  vs.  $\delta$  curve and formula for  $\omega$  given earlier remain the same, at least to the neglect of the suction effect, despite the simplification. The suction is assumed to translate directly into a corresponding increase in the effective normal stress, and assuming friction coefficients  $\mu_B$  within the breakdown zone and  $\mu_F$  outside it, this causes the augmentation of shear resistance as shown in Fig. 9b.

Assuming that the augmented shear strength differs significantly from  $\tau_F$  only within a zone that is small compared to overall fault length, RICE [23] analysed the problem as if the shear distribution shown acted on a semi-infinite shear crack in plane strain and found that the breakdown zone size was (RICE [23], eq. (21))

$$\omega = \omega_0 [(1 + \beta^2)^{1/2} - \beta]^2,$$

where

$$\beta = \frac{3}{8} \frac{(-\Delta p)_{\max,0}}{\tau_B - \tau_F} [\mu_B(1 - \log 2) - \mu_F \log 2], \quad (37)$$

and where  $\omega_0$  is the value of  $\omega$  given by (34) and  $(-\Delta p)_{\max,0}$  corresponds to the quantity of (36) with  $\omega$  replaced by  $\omega_0$ . Further, the stress intensity factor  $k$ , based on excess of  $\tau_\infty$  over  $\tau_F$  as before, required to drive the slipping region against this augmented resistance, is (RICE [23], eq. (22))

$$k = \left(\frac{2\omega}{\pi}\right)^{1/2} \left\{ \frac{4}{3} (\tau_B - \tau_F) + (-\Delta p)_{\max} \left[ \mu_B + \frac{1}{2} \mu_F \log \left( \frac{4l}{e\omega} \right) \right] \right\}, \quad (38)$$

where  $e$  is the natural logarithm base, where the logarithm actually arises as the asymptotic form of a term which it closely approximates when  $l/\omega$  is greater than 2 or so, and where  $l$  is an outer cut-off dimension for the suction distribution. The latter arises because the slipping region has been modelled as being of semi-infinite extent and having spread at a steady speed for all prior time. This makes the expression for  $k$  unbounded, and the cut-off  $l$  can be regarded as the radius of the slipping region or, perhaps better, the distance over which the slipped region has spread at speeds which are of magnitude comparable to the current  $V$ . Fortunately, there is only a weak dependence on  $l$  (Table 4).

Table 4. Dependence of  $A$  on cut-off length  $l$

$l/\omega_0$	10	$10^2$	$10^3$
$A$ , for $\mu_F = 0.5 \mu_B$	1.26	1.69	2.11
$A$ , for $\mu_F = \mu_B$	1.88	2.74	3.59

Substituting (37) into (38) and neglecting higher powers of  $(-\Delta p)_{\max,0}/(\tau_B - \tau_F)$  than the first, one obtains

$$k = k_{\text{crit}} \left[ 1 + A \frac{\mu_B (-\Delta p)_{\max,0}}{(\tau_B - \tau_F)} \right] \quad (39)$$

or, using (36) and (34),

$$k = k_{\text{crit}} \left\{ 1 + \frac{4}{3\pi} A \frac{M}{G} \mu_B \frac{H}{\bar{\delta}} \left[ \frac{(1-\nu) G \bar{\delta} V}{(\tau_B - \tau_F) c} \right]^{1/2} \right\} \quad (40)$$

as the stress intensity factor required to drive the spreading region at speed  $V$ . Here

$$A = \frac{3}{8} \left[ \log(2e) + \frac{\mu_F}{\mu_B} \log(8l/e\omega_0) \right] \quad (41)$$

and  $k_{\text{crit}}$ , to which the above formula for  $k$  reduces when  $V = 0^+$ , is the same as in (1), namely the critical value that would be calculated by neglecting any pore-fluid effects:

$$k_{\text{crit}} = \left[ \frac{2G}{1-\nu} \mathfrak{G}_{\text{crit}} \right]^{1/2} = \left[ \frac{2G(\tau_B - \tau_F) \bar{\delta}}{1-\nu} \right]^{1/2}. \quad (42)$$

Table 4 shows that the factor  $A$  which enters (39), (40) is not strongly dependent on the cut-off length  $l$ . For example, recalling that  $\omega_0$  may be of the order 10 m for natural faults, the table covers a range from approximately 100 m to 10 km for  $l$ . For Table 5, which gives some results based on equation (40) for  $k$ ,  $A$  has been taken as 2 and the following choice of parameters has been made:  $\bar{\delta} = 2.5$  mm, which seems consistent with the COULSON results on natural granite joints reported by BARTON [2];  $c = 0.1$  m<sup>2</sup>/s, toward the larger end of the range suggested by well-head measurements

made near the location of recorded creep events on the San Andreas (KOVACH et al. [14]), but smaller than the ANDERSON and WHITCOMB [1] value of  $1 \text{ m}^2/\text{s}$ ;  $\mu_B = 0.7$ ;  $M/G = 3$ ;  $G = 200 \text{ kb}$ ;  $\tau_B - \tau_F = 100 \text{ b}$ , chosen toward the upper end of the seismic stress-drop range;  $\nu = 1/4$ ; and  $H/\delta = 1/5$ , which represents an average dilation angle of about  $8^\circ$  within the breakdown zone, and is rather toward the lower end of the extent of dilatancy reported in various cases by BARTON [2], [3]. These choices, all of which have some degree of arbitrariness, lead to

$$k = k_{\text{crit}} \left[ 1 + 0.23 \left( \frac{V}{\text{km/d}} \right)^{1/2} \right], \quad (-\Delta p)_{\text{max}} = 17 \left( \frac{V}{\text{km/d}} \right)^{1/2} \text{ bars}; \quad (43)$$

numerical results based on these expressions are given in Table 5.

Table 5. Increase with speed  $V$  of the maximum induced suction and the stress intensity factor  $k$  required to spread the slipping region; parameters chosen as in text

$V$ [km/d]	0 <sup>+</sup>	1	10	100
$(-\Delta p)_{\text{max}}$ [bars]	0	17	54	170
$k/k_{\text{crit}}$	1.0	1.23	1.73	3.30

The increases with  $V$  of the required  $k$  for fault spreading as shown in the table suggest that dilatant opening at the onset of slippage can be an important factor in stabilizing faults, causing slip to occur by creep rather than seismic motions. The speeds in the table cover the entire range of creep events reported by KING et al. [13] and most of these events fall in the 1 to 10 km/d range. The stress intensity required to drive the fault is seen to increase substantially in these ranges.

Presumably, the increase of  $k$  saturates at sufficiently high speed for two reasons. First, the induced suction may become sufficiently great that the liquid vaporizes or, perhaps more likely, that gases come out of solution, effectively cutting-off any further development of suction. Second, since the suction amounts to an increase in effective normal stress, the effect may ultimately be self-arresting because, as BARTON [3] shows, the amount of fault dilation decreases with increasing effective normal stress.

There is at present no reliable means of estimating this maximum possible  $k$ -value, but its significance for the earthquake mechanism is obvious. If the excess of  $\tau_\infty$  over  $\tau_F$  or the size of the slipping region becomes so large that  $k$ , e.g. as calculated from (31) or (32), exceeds this maximum value, then further quasi-static slippage is impossible and, instead, dynamic faulting must occur.

An upper estimate, although probably quite severely so, to this maximum  $k$  can be obtained by setting the maximum induced suction equal to the hydrostatic, or equilibrium, value of the pore pressure. The latter is 500 bars at a depth of 5 km, and equations (43) predicts a suction of this size when  $V = 865 \text{ km/d}$  (which is outside the range of the approximation that led to (39), (40)); the corresponding estimate of the upper bound to the maximum possible  $k$ -value is  $7.8 k_{\text{crit}}$ .

#### 4.2. Effects of Biot time-dependent elasticity on shear fault motion

As remarked in the general discussion of Section 2.3, and seen already for the inclusion model in Chapter 3, there are two means by which fluids can stabilize the rupture process and both apply to the spreading slip-region model of this portion of the

paper. Dilatant strengthening has just been discussed and the complementary effects of time-dependent BIOT elasticity, remarked upon in different ways for shear faults by NUR and BOOKER [21], BOOKER [5], RICE [23], and RICE and CLEARY [26], have been studied with the aid of a solution to the BIOT-coupled deformation-diffusion equations for a spreading shear fault by RICE and SIMONS [28].

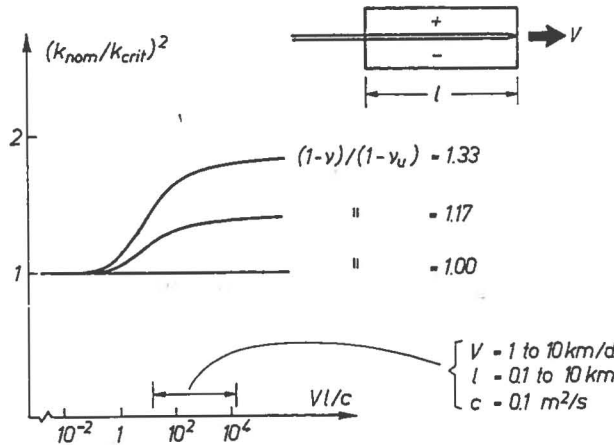


Fig. 10. The nominal stress intensity factor,  $k_{nom}$ , required to achieve  $k_{crit}$  at the tip of a plane-strain shear fault, uniformly loaded over distance  $l$ , that moves at steady speed  $V$  in a fluid-infiltrated elastic material (RICE and SIMONS [28]). Portion of axis marked corresponds to stable creep events (KING et al. [13], NASON and WEERTMAN [19]), assuming  $c$  as shown

Their solution pertains to a semi-infinite fault which is loaded in plane-strain conditions and which advances in a steady state with speed  $V$ , so that the deformation field seems fixed relative to an observer moving with the fault tip. The fault surfaces are shear-loaded by uniform tractions extending a fixed distance  $l$  behind the fault tip as indicated in Fig. 10, and these loadings are intended to simulate approximately the effect of an excess of  $\tau_{\infty}$  over  $\tau_F$  along a natural fault of length  $l$ , moving at instantaneous speed  $V$ .

We let  $k_{nom}$  be the "nominal" stress intensity factor in an ordinary elastic solid, without pore pressure effects, loaded identically to what is shown in Fig. 10. What RICE and SIMONS [28] find is that the solution to the coupled BIOT equations for the shear fault contains the same kind of characteristic inverse square-root stress singularity at the fault tip as in ordinary elasticity. Further, the pore pressure is found to vanish at the fault tip. Hence the near-tip singular field is of the same kind as could exist in a faulted solid under fully drained conditions, but it is found that the stress intensity factor  $k$  of this singular field is not the same as that, namely  $k_{nom}$ , for an identically loaded ordinary elastic solid, but is instead related to it by

$$k = k_{nom}h(Vl/c) . \tag{44}$$

The function  $h(\dots)$  which enters here is found to decrease from unity to  $(1 - \nu_u)/(1 - \nu)$  as its argument increases from 0 to  $\infty$ .

RICE and SIMONS [28] observe that since a region sufficiently near the fault tip always undergoes drained deformation, the simplest criterion for fault spreading, valid

when that region is large compared to the breakdown zone size, is to demand that  $k$  equal the critical value which would pertain under fully drained, ordinary elastic conditions, namely  $k_{\text{crit}}$  as given by (42). Thus, the criterion of fault motion is

$$k_{\text{crit}} = k_{\text{nom}} h(Vl/c) \quad \text{or} \quad k_{\text{nom}} = k_{\text{crit}}/h(Vl/c). \quad (45)$$

Hence  $k_{\text{nom}}/k_{\text{crit}}$  increases steadily with the spreading speed, from unity when  $V = 0$  to  $(1 - \nu)/(1 - \nu_u)$  when  $V$  becomes large. The term involving the POISSON ratios is the same as listed in column (i) of Table 1. The curves in Fig. 10, replotted from RICE and SIMONS [28], demonstrate the stabilizing effect. Of course, when the tectonic loading or extent of the slipped area is such that the nominal fault-tip  $k$ -value exceeds the maximum shown in the figure, quasi-static slippage is no longer possible according to the model, and the dynamic rupture must ensue.

Fig. 10 also shows the portion of the  $Vl/c$ -axis that corresponds to typical creep events reported by KING et al. [13] and by NASON and WEERTMAN [19], assuming a  $c$ -value within the range of the KOVACH et al. [14] well-head measurements. The ANDERSON and WHITCOMB [1]  $c$ -value, 10 times larger, would shift the data range one power of ten to the left. In either case it seems plausible that the observed creep slippage events are being stabilized, and hence made possible as quasi-static rather than dynamic events, at least in part, by the effects under discussion.

As remarked, the criterion (45) is sensible only if the effectively drained region at the fault tip is large compared to the breakdown zone size  $\omega$ . This will be so only if  $\omega$  is much less than  $c/V$ ; a more complete analysis, based on a simplification of the  $\tau$  vs.  $\delta$  relation of Fig. 8 to a simple form as in Fig. 9, was also carried out by RICE and SIMONS [28]. They find that for finite  $\omega/l$  the curves of Fig. 10 do not rise monotonically, but rather pass through a peak and decrease to an asymptotic value, at large  $Vl/c$ , which is the square root of the asymptote shown. Considering, for example, the uppermost curve in Fig. 10, rather than rising monotonically to 1.78, the curve peaks at approximately 1.58, 1.69, and 1.74 when  $\omega/l$  has the respective values of  $10^{-2}$ ,  $10^{-3}$ , and  $10^{-4}$ . The values  $Vl/c$  at these peaks are, respectively, 180, 625, and 2550. It may be presumed that the peaks mark instability points, since the  $k_{\text{nom}}$  vs.  $V$  relation decreases beyond them. That is, if no other stabilizing mechanism is operating simultaneously, the peak marks the largest possible  $k_{\text{nom}}$ -values and the largest possible speeds of fault creep. The interpretation of these results is discussed further by RICE and SIMONS [28].

It should be noted that there is no stabilizing effect of the kind considered in this section for a two-dimensional *anti*-plane strain fault model. In that case every element of the material deforms in pure shear, and no BIOT-like excess pore pressures are generated. Of course, the dilatant strengthening effect of the last section remains for anti-plane shear faults, and the appearance of the POISSON ratio in expressions for slip on *three*-dimensional faults (e.g., equations (11), (12)) suggests that these will show BIOT effects all around the fault border, including locations where the local deformation is of an anti-plane shear type.

##### 5. Localization into a shear zone

Chapter 3, based on the inclusion model, envisioned a more or less homogeneously deforming zone up to the moment of dynamic instability, whereas the limiting version of that model depicted in Fig. 3d and the considerations of Chapter 4 envision defor-

mations that are localized from the start in a fault zone. It remains an open question as to whether natural, versus laboratory, faulting ever or often involves significant inelastic deformation which occurs in a diffusely distributed mode that gradually concentrates into a localized shear band. Further, neither a constitutive formulation nor the theory as so far developed is suitable to examine localizations in materials undergoing rate-dependent inelastic deformation due, e.g., to the long-term surface-chemical effects discussed earlier.

Indeed, as explained briefly in Section 2.2.1 and in the recent review of the subject by the author (RICE [25]), the theory as studied thus far deals with materials having rate-insensitive incremental constitutive relations of the type

$$\dot{\sigma}_{ij} = L_{ijkl} \partial \dot{u}_k / \partial x_l, \quad (46)$$

where  $\sigma$ 's are stresses,  $u$ 's displacements,  $x$ 's cartesian co-ordinates fixed in space, where the superposed dots denote rates following material points, and where the incremental moduli  $L_{ijkl}$  vary with the history of deformation to the current deformed state and, generally, have a dependence on the "direction" of the velocity gradients as would distinguish elastic unloading from inelastic loading, or would make more complicated distinctions among inelastic loading directions, e.g. at a "yield vertex".

The localization bifurcation is addressed by considering a homogeneously deformed state and asking when the next increments of deformation need not be unique but, rather, can either continue the homogeneous deformation mode or bifurcate in a band-like mode, with stress rates and velocity gradients varying with position in the direction of some unit vector  $n$  as in Fig. 1 a. When such an  $n$  exists, the plane to which it is normal is said to be a plane of incipient localization (or "shear band"). The conditions which must be met for incipient localization are that velocity gradients anywhere within the band satisfy the kinematical condition

$$\partial \dot{u}_k / \partial x_l = (\partial \dot{u}_k / \partial x_l)^0 + g_k n_l, \quad (47)$$

where the  $g_k$  can be arbitrary functions of position in the direction of  $n$  and where the superscript 0 denotes the corresponding homogeneous field outside the band, and that for continuing equilibrium

$$n_i \dot{\sigma}_{ij} = n_i \dot{\sigma}_{ij}^0, \quad (48)$$

where again the 0 refers to the uniform outer field. Further, when the same constitutive moduli  $L_{ijkl}$  apply inside and outside the band at incipient localization, which can be shown to be the gravest case for a wide class of models of inelastic solids (RUDNICKI [30]), the condition reduces to the requirement that

$$(n_i L_{ijkl} n_l) g_k = 0 \quad (49)$$

has a non-trivial solution for the  $g$ 's. That is,

$$\det(n_i L_{ijkl} n_l) = 0 \quad (50)$$

when the quantity in parentheses is considered as a  $3 \times 3$ -matrix with indices  $j$  and  $k$ , and where "det" means "determinant of".

The theory was applied by RUDNICKI and RICE [32] to the simplest tensorial generalization, based on the first and second stress invariants, of the drained version of the pressure-sensitive, dilatant constitutive relation discussed in Section 3.1. This relation

is

$$\frac{1}{2}(\partial \dot{u}_i / \partial x_j + \partial \dot{u}_j / \partial x_i) = \frac{1}{2G} \dot{\sigma}'_{ij} + \frac{1}{9K} \delta_{ij} \dot{\sigma}'_{kk} + \frac{1}{h} \left( \frac{\sigma'_{ij}}{2\bar{\tau}} + \frac{\beta}{3} \delta_{ij} \right) \left( \frac{\sigma'_{kl}}{2\bar{\tau}} + \frac{\mu}{3} \delta_{kl} \right) \dot{\sigma}'_{ik}. \quad (51)$$

Here,  $G$ ,  $K$ ,  $h$ ,  $\mu$ , and  $\beta$  have the same interpretations as in 3.1,  $2\bar{\tau}^2 = \sigma'_{ij}\sigma'_{ij}$ ,  $\sigma'_{ij}$  denotes deviatoric stress, and  $\delta_{ij}$  is the KRONECKER (or unit) tensor. The stress rates are to be interpreted as "corotational" rather than ordinary material rates here, although the distinction is not essential for the results to be presented.

We note that when the dilational and frictional factors are related by  $\beta = \mu$ , the stress-strain relations are said to exhibit "plastic normality". Such cannot be expected to be a good approximation for rock deforming by frictional mechanisms and, indeed, experimental results when fitted to the above constitutive relation suggest that  $\beta$  and  $\mu$  differ, the former being the smaller.

Under fairly general conditions on the range of the constitutive parameters, RUDNICKI and RICE [32] find that localization can first occur in a program of deformation when the inelastic hardening modulus  $h$  has decreased to the critical value

$$h_{\text{crit}} = \frac{1 + \nu}{9(1 - \nu)} (\mu - \beta)^2 G - \frac{1 + \nu}{2} \left( 2P + \frac{\mu - \beta}{3} \right)^2 G, \quad (52)$$

where terms of order  $\bar{\tau}/G$  are neglected compared to unity, where  $\nu$  is the elastic POISSON ratio based on  $K$  and  $G$ , and where a version of the result given by RICE [26] is reported, in which  $P$  is the intermediate principal value of the tensor in parentheses immediately following  $1/h$  in (51). As such,  $P$  is some normalized measure of the intermediate principal value of the inelastic portion of the strain rate.

It is seen from (52) that whenever  $\mu$  differs from  $\beta$ , i.e., when "normality" does not apply, localization is possible under a *positive* hardening modulus  $h$  for some range of deformation states. This range includes always those states for which the inelastic deformation rates correspond to "plane strain", in the sense that the intermediate principal inelastic strain rate vanishes so that  $P = 0$ . Then

$$h_{\text{crit}} = \frac{(1 + \nu)^2}{18(1 - \nu)} (\mu - \beta)^2 G. \quad (53)$$

This is not, however, the gravest state, which occurs for  $P = -(\mu - \beta)/6$ .

On the other hand, the  $h_{\text{crit}}$  predicted by (52) is almost always large and negative ( $-0.3$  to  $-0.4 G$  for representative  $\mu$  and  $\beta$ ) in axi-symmetric compression.

This review of results may be sufficient to emphasize that large-scale post-peak strain-softening behavior, as envisioned in some precursory concepts, can be expected to exist without some degree of localization only in very special deformation states, and for the most common plane-strain-like tectonic deformations, localization could occur before peak conditions are attained. Some additional topics which need more study in this connection include localization behavior based on "vertex-like" yield models, which RUDNICKI and RICE [32] and RUDNICKI [29] argue to be rather generally implied by concepts of frictional slip on microcracks, the role of small initial non-uniformities of material properties in concentrating deformation (e.g., RICE [25]), and, of course, the generalization of the theory to a wide class of rate-sensitive constitutive relations.

### 6. Conclusion

A wide variety of models for processes precursory to earthquake rupture have been reviewed. The study is organized around failure modes involving localization, deformation to "runaway" instability of an inhomogeneous zone, representing either a "weakened" or a seismic gap zone, and the spread of slipping regions along pre-existing faults. One of the least satisfactory elements of current theory is the lack of suitable inclusion in constitutive relations, for rock masses or for fault slip, of long-term time-dependent effects, presumably of a surface-chemical origin, and involving time-dependent crack weakening as well as cementation at contacts.

It is emphasized that a general precursor for all types of rupture models, and particularly inclusive of those based on time-independent material models, is the acceleration of local deformations relative to remote tectonic deformations as critical conditions for instability are approached. Some constraints suggested by the models on the nature and spatial extent of large-scale precursory dilatancy are discussed.

Further, it is argued on the basis of some mechanically consistent, quantitative models of rupture processes that the mechanical interactions between a rock mass and infiltrating pore fluids can give rise to distinctive short-time precursors. These effects arise from the complementary processes of dilatant hardening in non-elastic deformation, and of time dependence of effective elastic stiffness due to BIOT coupling of deformation and diffusion. Both serve to stabilize rock masses and fault zones against abrupt failure, giving rise instead to periods of creep that may, sometimes, be accelerating precursors to dynamic rupture, and that may sometimes allow the completely quasi-static, rather than dynamic, relief of tectonic loading.

This paper was prepared under support of the NSF Geophysics Program and the USGS Earthquake Hazards Reduction Program. I am grateful to V. I. MYACHKIN for encouraging its preparation and to M. P. CLEARY, J. W. RUDNICKI, and D. A. SIMONS for various discussions relating to its theme.

### References

- [1] ANDERSON, D. L., and J. H. WHITCOMB, Time-Dependent Seismology. *J. geophys. Res.* *80* (1975), 718—732.
- [2] BARTON, N., Review of a New Shear-Strength Criterion for Rock Joints. *Engin. Geol.* *7* (1973), 287—332.
- [3] —, The Shear Strength of Rock and Rock Joints. *Internat. J. Rock Mech. and Min. Sci.* *13* (1976), 255—279.
- [4] BIOT, M. A., General Theory of Three Dimensional Consolidation. *J. appl. Phys.* *12* (1941), 155—164.
- [5] BOOKER, J. R., Pore Pressure and Strain. In: *Proc. Conf. on Tectonic Problems in the San Andreas Fault System*, ed. by R. L. KOVACH and A. NUR, Stanford 1973, 446—452.
- [6] BRACE, W. F., and R. J. MARTIN, A Test of the Law of Effective Stress for Crystalline Rocks of Low Porosity. *Internat. J. Rock Mech. and Min. Sci.* *5* (1968), 415—436.
- [7] —, PAULDING, B. W., and C. H. SCHOLZ, Dilatancy in the Fracture of Crystalline Rocks. *J. geophys. Res.* *71* (1966), 3939—3953.
- [8] BUDIANSKY, B., and R. J. O'CONNELL, Elastic Moduli of Cracked Solids. *Internat. J. Solids and Struct.* *12* (1976), 81—97.
- [9] DIETERICH, J. H., Time-Dependent Friction in Rocks. *J. geophys. Res.* *77* (1972), 3690—3697.
- [10] —, Time-Dependent Friction and the Mechanics of Stick-Slip. *Pure and appl. Geophys.* ■■■ 1977 (in press).
- [11] FRANK, F. C., On Dilatancy in Relation to Seismic Sources. *Rev. Geophys. and Space Phys.* *3* (1965), 485—503.

- [12] JAEGER, J. C., and N. G. W. COOK, *Fundamentals of Rock Mechanics*, 2nd ed. London 1976.
- [13] KING, C.-Y., NASON, R. D., and D. TOCHER, Kinematics of Fault Creep. *Philos. Trans. roy. Soc. London A* 274 (1973), 355—360.
- [14] KOVACH, R. L., NUR, A., WESSON, R. L., and R. ROBINSON, Water-Level Fluctuations and Earthquakes on the San Andreas Fault Zone. *Geology* 3 (1975), 437—440.
- [15] MARTIN, R. J., Time-Dependent Crack Growth in Quartz and its Application to the Creep of Rocks. *J. geophys. Res.* 77 (1972), 1406—1419.
- [16] — and W. B. DURHAM, Mechanics of Crack Growth in Quartz. *J. geophys. Res.* 80 (1975), 4837—4844.
- [17] MYACHKIN, V. I., KOSTROV, B. V., SOBOLEV, G. A., and O. G. SHAMINA, Experimental and Theoretical Investigations of Processes that are Possible Forerunners of Earthquakes (in Russian). *Izv. AN SSSR, Fiz. Zemli* 10 (1974), 107—112.
- [18] —, SOBOLEV, G. A., DOLBILKINA, N. A., MOROZOV, V. N., and V. B. PREOBRAZHENSKY, The Study of Variations in Geophysical Fields Near Focal Zones of Kamchatka. *Tectonophysics* 14 (1972), 287—293.
- [19] NASON, R., and J. WEERTMAN, A Dislocation Theory Analysis of Fault Creep Events. *J. geophys. Res.* 78 (1973), 7745—7751.
- [20] NUR, A., Dilatancy, Pore Fluids, and Premonitory Variations of  $t_s/t_p$  Travel Times. *Bull. seism. Soc. Amer.* 62 (1972), 1217—1222.
- [21] — and J. R. BOOKER, Aftershocks Caused by Pore Fluid Flow? *Science* 179 (1972), 885—887.
- [22] PALMER, A. C., and J. R. RICE, The Growth of Slip Surfaces in the Progressive Failure of Overconsolidated Clay. *Proc. roy. Soc. London A* 332 (1973), 527—548.
- [23] RICE, J. R., The Initiation and Growth of Shear Bands. In: *Plasticity and Soil Mechanics*, ed. by A. C. PALMER, Cambridge (Engl.) 1973, 263—274.
- [24] —, On the Stability of Dilatant Hardening for Saturated Rock Masses. *J. geophys. Res.* 80 (1975), 1531—1536.
- [25] —, The Localization of Plastic Deformation. In: *Theoretical and Applied Mechanics (Proc. 14th IUTAM Congr., Delft, 1976)*, ed. by W. T. KOITER, Vol. 1, Amsterdam 1976, 207—220.
- [26] — and M. P. CLEARY, Some Basic Stress-Diffusion Solutions for Fluid-Saturated Elastic Porous Media with Compressible Constituents. *Rev. Geophys. and Space Phys.* 14 (1976), 227—241.
- [27] —, RUDNICKI, J. W., and D. A. SIMONS, Deformation of Spherical Cavities and Inclusions in Fluid-Infiltrated Elastic Solids. *Internat. J. Solids and Struct.* (submitted for publ., 1977).
- [28] — and D. A. SIMONS, The Stabilization of Spreading Shear Faults by Coupled Deformation-Diffusion Effects in Fluid-Infiltrated Porous Materials. *J. geophys. Res.* 81 (1976), 5322—5334.
- [29] RUDNICKI, J. W., The Effect of Stress-Induced Anisotropy on a Model of Brittle Rock Failure as Localization of Deformation. In: *Proc. 18th U.S. Symp. on Rock Mechanics, Keystone (Col.)*, June 1977 (in press).
- [30] —, Localization of Deformation, Brittle Rock Failure, and a Model for the Inception of Earth Faulting. Thesis, Brown Univ., Providence (R. I.) 1977.
- [31] —, The Inception of Faulting in a Rock Mass with a Weakened Zone. *J. geophys. Res.* 82 (1977), 844—854.
- [32] — and J. R. RICE, Conditions for the Localization of Deformation in Pressure-Sensitive Dilatant Materials. *J. Mech. and Phys. Solids* 23 (1975), 371—394.
- [33] SCHOLZ, C. H., Static Fatigue of Quartz. *J. geophys. Res.* 77 (1972), 2104—2114.
- [34] —, SYKES, L. R., and Y. P. AGGARWAL, Earthquake Prediction: A Physical Basis. *Science* 181 (1973), 803—810.
- [35] STUART, W. D., Diffusionless Dilatancy Model for Earthquake Precursors. *Geophys. Res. Lett.* 1 (1974), 261—264.
- [36] —, Strain Softening Fault Dynamics Prior to Earthquakes. *J. geophys. Res.* (submitted for publication, 1977).
- [37] SUNDARAM, P. N., GOODMAN, R. E., and C. Y. WANG, Precursory and Coseismic Water-Pressure Variations in Stick-Slip Experiments. *Geology* 4 (1976), 108—110.
- [38] SWOLFS, H. S., Chemical Effects of Pore Fluids on Rock Properties. In: *Underground Waste Management and Environmental Implications*, ed. by T. D. COOK (Amer. Assoc. Petrol. Geol., Mem. 18), Tulsa 1972, 224—234.

- [39] WACHTMAN, J. B., Highlights of Progress in the Science of Fracture of Ceramics and Glass. *J. amer. ceram. Soc.* 57 (1974), 509—519.
- [40] WAWERSIK, W. R., and W. F. BRACE, Post-Failure Behavior of Granite and Diabase. *Rock Mech.* 3 (1971), 61—85.
- [41] — and C. FAIRHURST, A Study of Brittle Rock Failure in Laboratory Compression Experiments. *Internat. J. Rock Mech. and Min. Sci.* 7 (1970), 561—575.
- [42] WHITCOMB, J. H., GARMAN, J. D., and D. L. ANDERSON, Earthquake Prediction: Variation of Seismic Velocities before the San Fernando Earthquake. *Science* 180 (1973), 632—635.
- [43] WIEDERHORN, S. M., Influence of Water Vapor on Crack Propagation in Soda-Lime Glass. *J. amer. ceram. Soc.* 50 (1967), 407—414.

